

FILE COPY



**US Army Corps  
of Engineers**

Construction Engineering  
Research Laboratory

USACERL TECHNICAL REPORT M-89/15  
September 1989  
Electromagnetic Pulse (EMP) Validation  
and Design Recommendations for C<sup>3</sup>I Facilities

②

**AD-A213 825**

## **Arc-Sprayed Coatings for Electromagnetic Pulse Protection: Assessment of Physical and Electrical Properties**

by  
Howard S. Savage  
Ray G. McCormack

The Army is studying methods of protecting sensitive electronic equipment against electromagnetic pulse (EMP) and radiofrequency interference (RFI) events. Part of this work focuses on metal arc-spray techniques as a potentially low-cost alternative to traditional EMP/RFI protection. Arc-sprayed metal coatings have been used for several years in different applications; however, little is known about the physical and electrical properties of these coatings. A better understanding of these properties would allow spraying parameters to be optimized, ensuring the most effective coating at the lowest cost.

In this study, aluminum, aluminum bronze, copper, low-carbon steel, 13 percent chrome steel, nickel, nickel chrome, tin, and zinc were sprayed onto paper and aluminum foil substrates using the two-wire arc-spray process to determine the physical and electrical characteristics of these materials when sprayed on ordinary rooms composed of common construction materials. Zinc was found to be the most economical material and produced the least amount of substrate degradation. Quantities observed include: deposition efficiency; size of conductive area formed; size of opaque area formed; thickness required for opacity; and radius of curvature of a free-standing coating at fracture.

Simple models were used to calculate: (1) the minimum radius of curvature to which a free-standing coating of given thickness could be bent without causing fracture; (2) the maximum possible droplet temperatures from power input considerations; and (3) the maximum stable droplet size at the source based on spraying pressure and surface tension. Several of the coatings were also assessed using scanning electron microscopy (SEM).

Approved for public release; distribution is unlimited.

NTIC  
OCT 3 9 1989

89 10 20 174

UNCLASSIFIED  
SECURITY CLASSIFICATION OF THIS PAGE

REPORT DOCUMENTATION PAGE				Form Approved OMB No 0704-0188 Exp Date Jun 30 1986	
1. REPORT SECURITY CLASSIFICATION <b>UNCLASSIFIED</b>			1b. RESTRICTIVE MARKINGS		
2. SECURITY CLASSIFICATION AUTHORITY			3. DISTRIBUTION AVAILABILITY OF REPORT Approved for public release; distribution is unlimited.		
2b. DECLASSIFICATION/DOWNGRADING SCHEDULE			5. MONITORING ORGANIZATION REPORT NUMBER(S)		
4. PERFORMING ORGANIZATION REPORT NUMBER(S) USACERL TR M-89/15			5. MONITORING ORGANIZATION REPORT NUMBER(S)		
6a. NAME OF PERFORMING ORGANIZATION U.S. Army Construction Engr Research Laboratory		6b. OFFICE SYMBOL (If applicable) CECER-EM		7a. NAME OF MONITORING ORGANIZATION	
6c. ADDRESS (City, State, and ZIP Code) P.O. Box 4005 Champaign, IL 61827-4005		7b. ADDRESS (City, State, and ZIP Code)			
8a. NAME OF FUNDING SPONSORING ORGANIZATION HQUSACE		8b. OFFICE SYMBOL (If applicable)		9. PROCUREMENT INSTRUMENT IDENTIFICATION NUMBER	
8c. ADDRESS (City, State, and ZIP Code) 20 Massachusetts Ave, NW. Washington, DC 20314		10. SOURCE OF FUNDING NUMBERS			
		PROGRAM ELEMENT NO 4A162734		PROJECT NO AT41	TASK NO CO
				WORK UNIT ACCESSION NO 054	
11. TITLE (Include Security Classification) Arc-Sprayed Coatings For Electromagnetic Pulse Protection: Assessment of Physical and Electrical Properties (Unclassified)					
12. PERSONAL AUTHOR(S) Savage, Howard S. and McCormack, Ray G.					
13a. TYPE OF REPORT Final		13b. TIME COVERED FROM _____ TO _____		14. DATE OF REPORT (Year, Month, Day) 1989, September	
15. PAGE COUNT					
16. SUPPLEMENTARY NOTES Copies are available from the National Technical Information Service, 5285 Port Royal Road, Springfield, VA 22161.					
17. COSATI CODES			18. SUBJECT TERMS (Continue on reverse if necessary and identify by block number)		
FIELD	GROUP	SUB-GROUP	arc spraying coatings, electromagnetic pulses radiation shields		
09	07				
19. ABSTRACT (Continue on reverse if necessary and identify by block number) <p>The Army is studying methods of protecting sensitive electronic equipment against electromagnetic pulse (EMP) and radiofrequency interference (RFI) events. Part of this work focuses on metal arc-spray techniques as a potentially low-cost alternative to traditional EMP/RFI protection. Arc-sprayed metal coatings have been used for several years in different applications; however, little is known about the physical and electrical properties of these coatings. A better understanding of these properties would allow spraying parameters to be optimized, ensuring the most effective coating at the lowest cost.</p> <p>In this study, aluminum, aluminum bronze, copper, low-carbon steel, 13 percent chrome steel, nickel, nickel chrome, tin, and zinc were sprayed onto paper and aluminum foil substrates using the two-wire arc-spray process to determine the physical and electrical characteristics of these materials when sprayed on ordinary rooms composed of common construction materials. Zinc was found to be the most economical material and produced the least amount of substrate degradation. Quantities observed include: deposition efficiency; size of conductive area formed; size of opaque area formed; thickness required for opacity; and radius of curvature of a free-standing coating at fracture.</p> <p style="text-align: right;">(Cont'd)</p>					
20. DISTRIBUTION AVAILABILITY OF ABSTRACT Full Text Available <input checked="" type="checkbox"/> Data Only <input type="checkbox"/> Unavailable			21. ABSTRACT SECURITY CLASSIFICATION <b>UNCLASSIFIED</b>		
22. NAME OF PERSON/ORGANIZATION Dana Finney			23. TELEPHONE (Include Area Code) (217) 352-6511 (X389)		24. OFFICE SYMBOL CECER-INT-E

UNCLASSIFIED

Block 19 (con't)

Simple models were used to calculate: (1) the minimum radius of curvature to which a free-standing coating of given thickness could be bent without causing fracture; (2) the maximum possible droplet temperatures from power input considerations; and (3) the maximum stable droplet size at the source based on spraying pressure and surface tension. Several of the coatings were also assessed using scanning electron microscopy (SEM).

UNCLASSIFIED

## FOREWORD

This work was performed for the Directorate of Engineering and Construction, Headquarters, U.S. Army Corps of Engineers (HQUSACE), under Project 4A162734AT41, "Military Facilities Engineering Technology"; Work Unit CO-054, "Electromagnetic Pulse (EMP) Validation and Design Recommendations for C'I Facilities." The HQUSACE Technical Monitor was R. Wells, CEEC-EE.

The investigation was performed by the Engineering and Materials Division (EM), U.S. Army Construction Engineering Research Laboratory (USACERL). Dr. Robert Quattrone is Chief of EM. The USACERL technical editor was Dana Finney, Information Management Office.

The authors appreciate the support from other USACERL-EM personnel during this project: Peter Williams provided assistance with arc-spraying techniques and computer plotting; Robert Weber cooperated in the scanning electron microscopy work; and Tim Race provided access to the Paint Laboratory equipment. Administrative help from Tracy Wilson is also acknowledged.

COL. Carl O. Magnell is Commander and Director of USACERL, and Dr. L. R. Shaffer is Technical Director.



**A-1**

## CONTENTS

	Page
DD FORM 1473	1
FOREWORD	3
LIST OF TABLES AND FIGURES	5
<b>1 INTRODUCTION</b> .....	9
Background	9
Objective	10
Approach	10
Scope	10
Mode of Technology Transfer	11
<b>2 EXPERIMENTAL PROCEDURE</b> .....	12
Technology Overview	12
Experimental	12
<b>3 RESULTS AND DISCUSSION</b> .....	17
Aluminum	17
Aluminum Bronze	20
Copper	23
Iron (Low-Carbon Steel)	26
13 Percent Chrome Steel (AS21)	29
Nickel	31
Nickel-Chrome	33
Tin	33
Zinc	37
<b>4 SUMMARY OF FINDINGS</b> .....	64
Deposition Parameters	64
Deposited Mass	64
Deposit Efficiency	64
Radius of Conductivity	65
Radius of Opacity	65
Opacity Thickness	65
Bend Testing	65
SEM Observations	65
Wire Feed Rate Measurements	66
Maximum Droplet Temperature Calculation	66
Maximum Stable Droplet Size Calculation	67
Consumption Calculation	67
<b>5 CONCLUSIONS AND RECOMMENDATIONS</b> .....	69
<b>REFERENCES</b>	71
<b>APPENDIX: Various Deposition Parameters Identified for the Study</b>	73
<b>DISTRIBUTION</b>	

## TABLES

Number		Page
1	Wire Feed Rate Measurements for Aluminum	19
2	Wire Feed Rate Measurements for Aluminum Bronze	22
3	Wire Feed Rate Measurements for Copper	25
4	Wire Feed Rate Measurements for Iron (Low-Carbon Steel)	28
5	Wire Feed Rate Measurements for 13 Percent Chrome Steel	30
6	Wire Feed Rate Measurements for Nickel	32
7	Wire Feed Rate for Nickel-Chromium Alloy	34
8	Spraying Parameters for Zinc Tests	38
9	Deposited Mass (g) for Zinc Coatings Sprayed Onto Graph Paper	40
10	Deposit Efficiency for Zinc Under Varied Spray Conditions	42
11	Radius of Conductivity (cm) for Zinc	43
12	Radius of Opacity (cm) for Zinc	45
13	Opacity Thickness (cm) for Zinc	47
14	Bend Test Results for Zinc (AS14)	48
15	Wire Feed Rate for Zinc	62
16	Temperature (K) at Different Vapor Pressures	67
17	Material Consumption and Cost	68

## FIGURES

Number		Page
1	"Lateral Breeze" Generation Which Gives Rise to Droplet Motion Parallel to the Substrate Surfaces at Locations Away From the Spray Center	36
2	SEM Micrograph of Zinc Arc-Sprayed at a Distance of 15 cm	50

## FIGURES (Cont'd)

Number		Page
3	Highly Magnified Image of Arc-Sprayed Zinc Near Spray Center (Region A in Figure 2)	51
4	Highly Magnified Image of Arc-Sprayed Zinc (Region B in Figure 2)	52
5	Highly Magnified View of Arc-Sprayed Zinc (the Column in Figure 4)	52
6	Highly Magnified Image of Arc-Sprayed Zinc (Region C in Figure 2)	53
7	Highly Magnified Image of Arc-Sprayed Zinc (Closer View of Figure 6)	53
8	High Magnification of Arc-Sprayed Zinc (Region D in Figure 2)	54
9	Deposit Droplet Shape	54
10	SEM Micrograph Showing Interfacial Surface of Arc-Sprayed Zinc After Delamination From Aluminum Foil Substrate	55
11	SEM Micrograph Showing Bottom Surface of Arc-Sprayed Zinc Coating Adjacent to Spray Center	56
12	SEM Micrograph of Arc-Sprayed Zinc Droplets Deposited Far From Spray Center Showing Reproduction of Substrate Topography	56
13	SEM Micrograph of Arc-Sprayed Zinc Droplets Showing Shrinkage and Conformation to Substrate Topography	57
14	SEM Micrograph of Fracture Surface in Arc-Sprayed Zinc Approximately 1.9 cm From the Spray Center for a Spray Distance of 15 cm	58
15	Higher Magnification of the Arc-Sprayed Zinc Region in Figure 14	58
16	SEM Micrograph of Arc-Sprayed Zinc Approximately 2.5 cm From the Spray Center for a Spray Distance of 15 cm	59
17	SEM Micrograph of Arc-Sprayed Zinc Away From the Spray Center at a Spraying Distance of 61 cm	59
18	SEM Micrograph of Arc-Sprayed Zinc at a Spray Distance of 15 cm for a Region Similar to That in Figure 17	60

## FIGURES (Cont'd)

Number		Page
19	SEM Micrograph of Arc-Sprayed Zinc at a Spraying Distance of 61 cm (Similar to Region in Figure 17, Showing Greater Detail)	61
20	Detail of Droplet in Figure 19 at Higher Magnification	61

# ARC-SPRAYED COATINGS FOR ELECTROMAGNETIC PULSE PROTECTION: ASSESSMENT OF PHYSICAL AND ELECTRICAL PROPERTIES

## 1 INTRODUCTION

### Background

Electromagnetic shielding of structures is achieved by surrounding the volume to be shielded with a mechanically and electrically continuous conductive material. The U.S. Army Construction Engineering Research Laboratory (USACERL) has conducted long-term research into military applications of electromagnetic shielding, which include:<sup>1</sup> (1) protection of sensitive electronic equipment from external interference; (2) prevention of compromising emanations from equipment processing classified information; and (3) shielding sensitive and strategic electronics from the effects of electromagnetic pulse (EMP). Electrical conductivity of the shielding material is the single most important parameter affecting the shielding effectiveness of a structure; regions of low electrical conductivity or discontinuity such as joints, cracks, and seams contribute to reduced shielding performance.

Typical shielded structures have been constructed by bolting or welding metal sheets, panels, and modules. Bolted structures tend to provide a lower degree of shielding than all-welded structures. The leakiness of bolted structures arises from the mechanical joints where oxides inhibit electrical continuity of the joint. Electrical discontinuities at the joints of bolted structures are aggravated by surface and shape imperfections in the joint materials and the buildup of corrosion products with time due to normal atmospheric corrosion of the materials. Bolted construction also can be expensive and provides only limited flexibility for retrofitting existing structures with EMP shielding. Welded structures tend to provide a high degree of EMP shielding because metallurgical joining of the metal sheets at the joint ensures complete mechanical and electrical continuity. Welded structures for EMP protection are material consumers because the sheet thickness required for good weldability is in excess of that required to provide adequate EMP shielding. Welded construction tends to be expensive but provides more flexibility in retrofitting existing structures for shielding than do bolted structures.

Plastic is most often used to manufacture housings for electronic equipment due to its low material and fabrication costs relative to metals. However, plastics and many other common low-cost construction materials lack the inherent EMP shielding properties of metals. Metal-arc spraying has become an accepted technique for imparting shielding properties to plastic housings at a low cost; spraying room-size structures of standard or low-cost construction materials to impart shielding is a logical extension of this successful technology.<sup>2</sup>

The arc-spray process in simplest form consists of bringing together a pair of consumable wire electrodes to form an arc and then propelling the resulting molten metal from the wires onto a substrate using a stream of compressed gas or some other mechanism. Although the arc-spray operator has a degree of control over some of the spraying parameters (e.g., wire feed rate, arc voltage, wire composition), there is a much larger number of dependent and independent variables, all of which

---

<sup>1</sup>P. Nielson, *Electromagnetic Shielding of Full-Sized Structures by Metal Arc Spraying*, Technical Report M-332/ADA132883 (U.S. Army Construction Engineering Research Laboratory [USACERL], August 1983).

<sup>2</sup>P. Nielsen.

interact to affect the properties of the deposit. At present, little is known about the effect of these variables on coating quality.

For EMP shielding of construction materials, it is important to know how deposition parameters affect the electrical and physical properties of the coating as well as the interface between the coating and the substrate. For practical shielding applications, it is desirable to form a maximal conductive area with an acceptable deposition efficiency. By understanding how these parameters influence the coating deposited, spraying conditions can be optimized to produce the best shielding at the lowest relative cost.

## Objective

The objectives of this work were to assess the physical and electrical properties of different arc-sprayed coatings to optimize spraying parameters for application in shielding military structures against EMP and related phenomena. The specific objectives of this study were to: (1) determine which of the available metal wires are generally suitable for spraying onto organic construction materials; (2) determine how some of the controllable spraying parameters interact with properties of the deposit; and (3) observe the effects of some of the controllable spraying parameters on the structure of the deposited material using scanning electron micro-copy (SEM).

## Approach

All tests were conducted in-house at USACERL. The study proceeded as follows:

1. Zinc was sprayed, using a large number of variations in spraying parameters, onto graph paper substrates supported with masonite to determine the effects of the spraying parameters on deposit properties. This information was assessed to determine which trends in the spraying parameters produced an optimal deposit with minimal substrate degradation.
2. The information on trends in spraying parameters for deposit optimization was extended to the other test materials when spraying them onto graph paper substrates for deposit evaluation.
3. Several of the materials were sprayed onto aluminum foil concurrently with spraying onto graph paper for SEM observation.
4. Several materials were sprayed onto brick and qualitatively evaluated for performance.
5. Zinc was sprayed onto a series of low-cost construction materials and qualitatively evaluated.

## Scope

This study determined only some of the interactions between controllable arc-spraying parameters and the nature of the deposit for coatings sprayed onto paper substrates with no relative motion between the spray gun and the substrate. Metals sprayed were limited to aluminum, aluminum bronze, copper, low-carbon steel, nickel, nickel-chromium, 13 percent chromium steel, tin, and zinc. Use of controlled relative motion between the source and substrate, if it had been available, would have obscured some of the results that were obtained without it.

### Mode of Technology Transfer

Arc spray in shielding applications was demonstrated successfully as part of the FY88 Facilities Technology Application Test (FTAT) program (which has now become the Facilities Engineering Applications Program [FEAP]). Two rooms targeted for TEMPEST protection were arc-sprayed with zinc at Fort Devens, MA (a technical report is in preparation.) From the demonstration, it is anticipated that the U.S. Army Corps of Engineers (USACE) will adopt this shielding approach for some applications. Information gathered in this study will be used in preparing appropriate guidance for implementing arc-spray technology in the field; it will ultimately be incorporated into Technical Manual 5-855-5, *Electromagnetic Pulse Protection*, which is being revised. Further, this information will serve as a knowledge base for an ongoing study into relative motion between spray source and substrate.

## 2 EXPERIMENTAL PROCEDURE

### Technology Overview

Thermally sprayed coatings have been used for many years in applications such as corrosion and wear prevention; however, only in the past few years has significant interest grown in applying thermally sprayed coatings to radiofrequency interference (RFI)/electromagnetic interference (EMI) shielding. Thermal spraying in general consists of heating the material to be deposited to a suitable temperature and then projecting it onto the substrate. Deposition over large substrate areas is achieved by relative motion of the spray source and the substrate using a process similar to spray-painting.

The arc-spray process uses a pair of wires both as electrodes to supply heat and as source material to be projected onto the substrate by a stream of compressed gas or other mechanism. In simplest form, arc-spraying consists of bringing two electrodes (wires) together to strike an arc and blasting the arc with a high-velocity gas stream to propel droplets of molten metal off the wires as they are melted. Important deposition parameters include: spraying pressure (gas stream velocity), wire feed pressure (wire feed rate), arc voltage, arc current, spraying time, spraying distance, substrate surface roughness, distance from center of spray pattern, substrate material, traverse speed, intertraverse distance, spraying gun position, ambient gas composition, humidity level, dew point, elastic constants of wire, friction of wire with handling assembly, spraying gas temperature, substrate temperature, substrate surface cleanliness, and substrate thickness.

One of the goals of this study was to determine the effect of such parameters on the deposit's properties. Coating characteristics of interest were: size of conductive area formed; size of opaque area formed; thickness of coating required for opacity; state of residual stress in the coating; deposition efficiency; and relative size of the conductive and opaque areas.

### Experimental

#### *Apparatus*

The arc-sprayer unit used to deposit the coatings tested in this work is a TAFA model 375 hand-held arc sprayer gun with a TAFA model 30.8A power supply. The power supply is rated at 28 V, 200 amps, for 100 percent duty cycle. The maximum open circuit voltage is 39 V. A 0.159-cm-diameter electrode/wire source material is supplied from spools mounted on the power supply. The wires are driven by a clamping gear-type device linked to an air motor in the sprayer gun. The sprayer unit was modified to allow the user to spray either compressed air or an externally supplied gas as propellant.

No suitable device was available for producing controlled, reproducible relative motion between the sprayer and the substrates, so it was decided that coatings would be sprayed at a fixed point on the substrates. Spraying at a fixed point allows observation of the variations in coating structure and deposition rate with distance from the spray center which would not be as visible if relative motion between the source and substrate were used.

As noted in Chapter 1, several of the arc-sprayed coatings were examined by SEM. The equipment used in those evaluations was an Amray model 1610 scanning electron microscope.

## *Materials*

Materials sprayed as coatings for this study included: zinc, aluminum bronze, low-carbon steel, 13 percent chrome steel, nickel, aluminum, tin, copper, and a nickel-chromium alloy. These metals were in the form of 0.159-cm-diameter wires supplied on spools by the manufacturer of the sprayer unit. Zinc wire was sprayed first and most extensively to develop trends since it is relatively inexpensive and easy to obtain.

## *Substrates*

Graph paper and aluminum foil were chosen as the primary substrate materials. The substrates were held in place during spraying by using binder clips to mount them to a masonite backing sheet. Graph paper was chosen as a substrate material for several reasons:

1. The ultimate goal of the process optimization study for which this work was done is to deposit, by an automated process, continuous conductive films onto the walls of ordinary rooms to provide EMI/RFI shielding. This means that the process must not cause charring or excessive thermal degradation of painted or paper-covered plasterboard and other surfaces. With paper substrates, it is possible to directly observe the thermal effects by looking at the back side of the paper.

2. Graph paper has grid marks that provide a convenient locational reference for some of the measurements that were made on the coatings.

3. Graph paper is nonconductive so as to provide minimal interference when making electrical measurements of the coating.

4. Graph paper is translucent, which allows coating pinhole porosity to be observed.

5. Unused graph paper has a consistently clean surface that requires no preparation.

Aluminum foil was chosen as a substrate material for the following reasons:

1. Aluminum is electrically conductive so as to provide an electrically continuous coating/substrate couple to minimize charging effects during SEM observation.

2. Foil has a consistently clean surface that requires no preparation.

3. Aluminum has a higher melting point than zinc; thus, melting of the aluminum foil would give some indication of the depositing material's temperature.

4. Aluminum foil is ductile enough to provide a record of particle impact without requiring the particle to stick.

Substrates sprayed with zinc for adhesion testing included: masonite, plasterboard, fiberglass paneling, plywood, and ceiling tile.

## *Deposition Parameters*

A long list of possible deposition and coating property variables was compiled (see the Appendix). Those considered relevant to this study are described under *Spraying Conditions* below.

## *Spraying Conditions*

Although the number of possible variables during spraying is very large as noted above, many are not independent and only a few are in the range of practical operator control. The variables determined to have a noticeable effect on the nature of the deposit in this work included: wire feed pressure, spray pressure, arc voltage, spray distance, spraying time, spraying gas composition, wire composition, substrate composition, substrate surface preparation, substrate geometry, temperature, and droplet size on impact with the substrate. Typical values of spray distance were 15, 30, 46, 61, 76, and 91 cm. Individual sets of conditions for the various materials sprayed were given labels such as ASxxxx where AS indicates "sprayed with air" and xxxx is a character code related to a specific set of conditions. These labels were assigned to facilitate data manipulation.

## *Measured Properties*

Deposited Mass. The mass deposited on the surface was determined by subtracting the mass of an uncoated substrate from that of a coated substrate.

Deposit Efficiency. The deposit efficiency was calculated by dividing the deposited mass by the mass of material sprayed. The mass of material sprayed was determined in most cases by spraying five (5) cent lengths of wire and then subtracting the mass of the material remaining in the gun after spraying (wires can be fed only up to the wire drivers) from that of the original length of wire.

Radius of Conductivity. The term "radius of conductivity" was developed to describe a characteristic dimension of the conductive area formed by the sprayed coating. The conductive area was mapped with an ohmmeter by probing for a center-to-edge resistance of 1 ohm and then plotting that point on another piece of graph paper (the coatings were sprayed on graph paper of the same size to simplify the location of coordinates). From the map of the boundary points, the coordinates of the four most extreme points in the x and y directions were averaged to give a center point. From the center point, the distance to each of the extreme points was calculated and averaged to give the "radius of conductivity." One ohm was chosen as a convenient reference value for three reasons:

1. The contact resistance and measurement noise for the ohmmeter probes was on the order of one-tenth of an ohm for most of the coatings.
2. Beyond the 1-ohm radius, the resistance of the coatings rises rapidly to infinity, often over distances of just a few millimeters.
3. Within the 1-ohm radius, the resistance of the coating drops rapidly into the minimum measurement range of 0.1-ohm contact resistance--again, often over distances of just a few millimeters.

It should be noted that these values are only representative of the stationary conditions used in making these coatings; the use of relative motion between the substrate and the sprayer and/or a nonnormal incidence will greatly affect these values.

Radius of Opacity. The "radius of opacity" was termed to describe the characteristic dimension of the region that appears free of porosity to the unaided eye. The boundaries of the region were determined by placing the coating/substrate (graph paper) composite onto a light box and locating the points closest to the spray center through which light passed. The spray pattern is usually not round. The maximum x and y widths were thus added and divided by 4 to give the average "radius of opacity" which allowed meaningful comparisons with the radius of conductivity.

Opacity Thickness. The term "opacity thickness" was developed to describe the characteristic coating thickness at the point of transition from an optically porous coating to an optically dense

coating at a distance of one radius of opacity from the spray center. The opacity thickness was taken as the average of the four thicknesses measured with a paint thickness tester at the points used to determine the radius of opacity.

Bend Testing. Bend testing was conducted to determine the radius of curvature necessary to cause fracture of a free-standing coating of given thickness. The coatings of known thickness were wrapped around mandrels of various diameters and the diameter of the mandrel that caused fracture was noted. The mandrel set used was model MG 1412 manufactured by Gardner Laboratory, Inc. Mandrel diameters were: 0.3175, 0.4763, 0.6350, 0.7938, 0.9525, 1.1113, 1.2700, 1.9050, and 2.54 cm. A simple model was developed to predict the minimum radius of bending that a free-standing coating could withstand without rupturing. The model makes three assumptions: (1) the coating is of uniform thickness, (2) the mid-thickness of the coating experiences zero strain, and (3) the coating ruptures when the outside radius is such that the strain is equal to or greater than a critical value "e." From the assumptions and geometry, an equation for the critical bending radius,  $r$ , in terms of the coating thickness,  $t$ , was derived:

$$r = t(1-e)/2e \quad [\text{Eq 1}]$$

Wire Feed Rate. Wire feed rate was measured to determine the effects of wire feed pressure, wire composition, and bending of the wire feed tubes on this rate. Measurements were made by shutting off the arc voltage, rotating the feed tips slightly so that the wires would not intersect, setting the spray pressure at 0.414 MPa, allowing the wires to feed for a fixed period of time (30 sec), and measuring the length of wire fed so that a rate could be determined. It should be noted that at wire feed pressures above about 0.483 MPa, noticeable loading of the air supply system occurred and it was necessary to have an assistant interactively adjust the wire feed pressure regulator to maintain the desired pressure.

Maximum Droplet Temperature Calculation. A simple model was developed to determine the maximum possible temperature of the sprayed droplets. Assumptions of the model include: (1) there is no oxidation reaction and (2) all power in the arc is used to heat the metal. Typical spraying parameters of wire feed rate, arc voltage, and arc current for each of the metals sprayed were used in the calculations.

Maximum Stable Droplet Size Calculation. The maximum stable droplet size was calculated from surface tension characteristics by assuming: (1) instability occurs when the applied external pressure exceeds the internal pressure due to the surface tension, (2) no oxidation reactions occur to modify the droplet surface tension, (3) the droplets have a spherical shape, (4) the pressure of the spraying gas acts only on the upwind side of the sphere such that the pressure on the downwind side of the sphere can be assumed to be zero (the pressure is a gauge pressure so the downwind gauge pressure is zero), and (5) the temperature of the droplet is the melting point of that particular material. The internal pressure,  $p$  (dynes per square centimeter), in the droplet due to the surface tension is given by:

$$p = 2T/r \quad [\text{Eq 2}]$$

where  $T$  is the surface tension in dynes per centimeter and  $r$  is the droplet radius in centimeters.

Setting the internal pressure equal to the spray pressure ( $1 \text{ psi} = 68947.6 \text{ dyne/cm}^2$ ), the maximum stable droplet dimension can be calculated as  $r = 2T/p$ . This value varies rapidly with spraying distance since the spraying pressure declines rapidly with distance from the nozzle and the effective pressure acting on the upwind side of the droplet varies as the droplet is accelerated and approaches the velocity of the spraying gas stream. The surface tension for most materials decreases with increasing temperature above the melting point; this property indicates that superheating of the droplets

will cause the maximum stable droplet size to be smaller. The calculation assumes static conditions; during subdivision in actual spraying, the melt viscosity will have a significant influence on the results.

Consumption Calculations. The power required to spray 1 cm<sup>3</sup> was calculated from the typical spraying parameters for that material (voltage, current, and wire feed rate). This number does not reflect the deposit efficiency, which decreases with increasing spray distance. The material cost per cubic centimeter was calculated using prices quoted from TAFE for 22.67 kg quantities of the materials on spools.

### 3 RESULTS AND DISCUSSION

The test results and a discussion for individual coating materials are presented for each type of wire evaluated. Similarities, differences, and general trends for all materials are summarized in Chapter 4.

#### Aluminum

##### *Deposition Parameters*

Aluminum was sprayed at 25 V, 200 amps, a wire feed pressure of 0.552 MPa, and a spray pressure of 0.414 MPa with air as the spraying gas (AS22).

##### *Deposited Mass*

The deposited mass was not measured. The high temperature of the depositing material burned holes through the paper and aluminum foil substrates. In one case for which aluminum was deposited successfully onto aluminum foil, the masonite backing material was badly charred. From these observations, it appears that aluminum arc-sprayed with air would not be a suitable shielding method since its application degrades organic materials on the surfaces to which it is applied. Oxidation of the droplet surface in flight probably inhibits droplet deformation on impact and thus inhibits adhesion to the substrate by (1) intimate contact between the molten metal and the substrate and (2) restricting mechanical interlocking between the droplets and the substrate topography. Because of the burning observed, the following tests were not completed: deposit efficiency, radius of conductivity, radius of opacity, opacity thickness, and bend testing.

##### *SEM Observations*

SEM images were not as clear as they could have been; there was definite evidence of charging effects due to the presence of an insulating oxide film on the surface of the particles. Several observations were made for aluminum sprayed onto aluminum foil at 15 cm:

1. At small droplet sizes, droplet topography is not strongly influenced by the substrate topography. This finding is possibly due to the relatively small area that can be covered by the small droplet compared with the size of the substrate features and the relatively large restraining tendency of an oxide film and surface tension on a small droplet. The rapid cooling (surface area-to-volume ratio) and smaller total heat capacity of the smaller droplets may also have an effect.

2. At intermediate droplet sizes, the droplet topography is influenced by the substrate topography. The surfaces of the droplets appear to mimic (poorly) the features of the substrate surface.

3. At large droplet sizes, the substrate topography is influenced by the droplet; localized melting under a significant portion of the droplet occurs.

4. The "lateral breeze" caused by air escaping from the spray center has a significant effect on the topography of some of the droplets deposited at about 5 cm from the spray center. Droplets in this region have microscopic edge features pushed radially outward from the macroscopic spray center.

5. There is a distinct "halo" visible on the substrate in the region surrounding widely spaced droplets. The exact nature of this halo is not known at this time; however, some possibilities include:

- The substrate is scoured locally by contact with the molten metal during droplet splattering.
- The shock wave associated with particle impact somehow disrupts the surface locally.
- Localized heating of the substrate by the molten droplet enhances atmospheric oxidation.
- The presence of the deposited particle causes a localized fluctuation in the "lateral breeze," thus reducing abrasion to the region by solidified particles carried in the airstream.
- The effect may be due to some combination of the above possibilities. Auger depth profiling in and away from the haloed regions would probably be the easiest way to interpret this finding.

#### *Wire Feed Rate Measurements*

Wire feed rate was measured during the tests and the results are listed in Table 1. In the table, "PF" indicates that problems were encountered when feeding the wire. With aluminum, the spools were fairly full and the presence of slack in the system near the spool often caused loops of wire to come off the spools. This problem was aggravated most by high wire-feed rates. A major improvement to the system would be to add some mechanism to dampen the jerky motion of the spools; perhaps some type of magnetic damping system similar to the ones used on fishing reels would be appropriate. In the events of bad feed on only one side, the measurement was not repeated and the average values are multiples of the length fed by one side.

The wire feed measurements show that the left side almost always fed slower than the right side and that the difference between the two was greatest for the b (bent) condition. The greater difference in the bent condition was due to the geometry of the sprayer unit which causes the left tube to have a smaller radius of curvature than the right; this condition leads to increased friction between the wire feed tube and the wire. The measurements clearly show that there was a significant difference between the wire feed rates in the straight and bent conditions at a given value of wire feed pressure. For a typical wire feed pressure value of 0.552 MPa during spraying, the difference was about 24.5 percent of the straight-tube value. Actual wire feed rates during spraying could reasonably be expected to be at some point between the two extremes.

#### *Maximum Droplet Temperature Calculation*

For the typical aluminum spraying parameters of 25 V, 200 amps, and 80 psi wire feed pressure (about 35.56 cm/sec total ft/min), there are about 16.97 kcal of heat available for each mole of material being sprayed. It takes 4.287 kcal to heat 1 mole of aluminum from room temperature to its melting point and 2.57 kcal to melt 1 mole of aluminum at 931 K. This leaves 10.11 kcal available to heat the liquid to 2375 K. This high temperature relative to the burning point of paper (about 500 K) and the melting point of aluminum explains why the arc-sprayed aluminum burned through paper and aluminum foil substrates and charred the masonite backing board. The strong tendency for aluminum to oxidize exothermically probably further increases the maximum possible droplet temperature.

Table 1  
Wire Feed Rate Measurements for Aluminum\*

wfp (MPa)	Meters Left**	Meters Right	Hose***	avec/s	tavec/s
0.6206	4.90	5.11	b	16.69	33.38
0.6206	6.31	6.31	s	21.03	42.06
0.5516	4.41	4.71	b	15.21	30.43
0.5516	6.03	6.05	s	20.13	40.28
0.4827	BF	4.38	b	14.61	29.21
0.4827	5.54	5.55	s	18.48	36.98
0.4137	BF	3.56	b	11.85	23.72
0.4137	4.99	5.00	s	16.66	33.32
0.3448	BF	3.01	b	10.03	20.07
0.3448	4.60	4.61	s	15.35	30.68
0.2758	BF	2.11	b	7.03	14.07
0.2758	3.90	3.92	s	13.04	26.06
0.2069	0.69	0.84	b	2.56	5.13
0.2069	3.01	3.04	s	10.07	20.17
0.1379	0	0	b	0	0
0.1379	2.00	2.02	s	6.70	13.41
0.1034	0	0	b	0	0
0.1034	1.44	1.45	s	4.81	9.60
0.0690	0	0	b	0	0
0.0690	0.74	0.75	s	2.49	4.98
0.0345	0	0	b	0	0
0.0345	0	0	s	0	0

\* wfp = wire feed pressure; avecms = average cm/sec for each wire; tavec/s = total average ft cm/sec of wire consumed during spraying.

\*\* BF = bad feed.

\*\*\* b = bent; s = straight.

### Maximum Stable Droplet Size Calculation

The maximum stable droplet size for aluminum was calculated for several spray pressures assuming a surface tension value of 860 dynes/cm. At 0.1034 MPa,  $r$  is  $1.66 \times 10^{-3}$  cm. At 0.4137 MPa,  $r$  is  $4.16 \times 10^{-4}$  cm. At 90 psi,  $r$  was  $2.77 \times 10^{-4}$  cm. The value for surface tension was taken from the *CRC Handbook of Chemistry and Physics*.<sup>3</sup>

### Consumption Calculations

The energy consumption was calculated to be about 7.1 kJ/cm<sup>3</sup> (1.97 W-hr/cm<sup>3</sup>). The material cost was \$5.41/kg, which is about \$0.0146/cm<sup>3</sup>.

## Aluminum Bronze

### Deposition Parameters

Aluminum bronze was sprayed at 25 V, 300 amps, a wire feed pressure of 20 psi, and a spray pressure of 0.6206 MPa. Air was used as the propellant gas. Holes were burned through the paper and aluminum substrates at a spray distance of 15 cm; therefore, the opacity thickness and bend tests were not conducted. However, substrate survivability was increased at larger spray distances.

### Deposited Mass

The deposited mass in grams for aluminum bronze (AS16) coatings sprayed onto graph paper was determined for each spray distance. The value of zero for a spray distance of 15 cm indicates that a hole burned through the graph paper and that the weight of the material deposited on the periphery of the hole was less than the mass of the paper removed in creating it. Results are as follow:

Spray distance (cm)	15	30	46	61	76
Deposited mass (g)	0.0	3.73	2.23	0.84	0.13

### Deposit Efficiency

The deposit efficiency was calculated using a value of 27.29 g for the sprayed mass. The results are as follow:

Spray distance (cm)	15	30	46	61	76
Deposit efficiency	0.0	0.14	0.08	0.03	0.01

### Radius of Conductivity

The radius of conductivity (ROC) for aluminum bronze was determined for each of the spray distances; the values are tabulated below. From these data, it can be seen that, as the spray distance increased, there was a tendency for the coating to become electrically discontinuous.

---

<sup>3</sup>R.C. Weast and M.J. Astle (Eds.), *CRC Handbook of Chemistry and Physics*, 63rd ed. (CRC Press, 1982-83).

Spray distance (cm)	15	30	46	61	76
ROC (cm)	2.5	4.2	3.9	0	0

### *Radius of Opacity*

No radius of opacity was measured. The sample sprayed at 30 cm would have had a sizable opaque area (still less than the ROC) except for the porosity at the center of the deposit. The sample sprayed at 46 cm showed pinhole porosity throughout.

### *SEM Observations*

SEM observations were made on a multilayer (multipass) coating that delaminated from a brick substrate due to thermal stresses and on the material sprayed at 15 cm. For the material sprayed at 15 cm (stationary), SEM observations seemed to indicate that aluminum bronze coatings fracture without large amounts of plastic deformation. The failure mode, even very near the spray center, appeared similar to the delamination observed in the zinc coatings distant from the spray center. Observations of the delaminated material indicated that there was some tendency for delamination to occur between individual layers of the coating during fracture. Observations of the sample's back side showed that the coating conformed very well to the topography of the brick and, when delamination occurred, there was a tendency for particles to be pulled out of the brick and remain embedded in the underside of the coating.

### *Wire Feed Rate Measurements*

Wire feed rate was measured and the results are listed in Table 2. Difficulties with wire feeding the aluminum bronze were minimal. The difference between wire feed rates for the bent and straight conditions at a given wire feed pressure were smaller for the aluminum bronze than for corresponding conditions in the aluminum wire tests. The wire feed rate for the aluminum bronze with the feed tubes bent was faster at all wire feed pressures than for the aluminum wire in the bent feed tubes at the same wire feed pressures. As in the case of the aluminum wire, the right side fed faster than the left, with the difference being more visible at higher wire feed pressures and using the bent condition.

### *Maximum Droplet Temperature Calculation*

Suitable thermodynamic data to do the calculation on this alloy could not be located. The lesser burning of graph paper by this material compared with the aluminum is probably a good indication that heating of the droplets by exothermic oxidation was not as significant.

### *Maximum Stable Droplet Size Calculation*

The maximum stable droplet size was not calculated because surface tension data for the alloy were not available.

### *Consumption Calculations*

The energy consumption was calculated to be about  $31.1 \text{ kJ/cm}^3$  ( $8.64 \text{ W-hr/cm}^3$ ). The material cost is \$11.58/kg which is about \$0.0910/cm<sup>3</sup>.

Table 2  
Wire Feed Rate Measurements for  
Aluminum Bronze\*

wfp (MPa)	Left (m)	Right (m)	Hose**	avecm/s	tavecm/s
0.6206	6.63	6.44	b	21.34	42.67
0.6206	6.92	6.95	s	23.11	46.23
0.5516	6.01	6.07	b	20.13	40.28
0.5516	6.55	6.58	s	21.88	43.79
0.4827	5.61	5.64	b	18.76	37.49
0.4827	6.05	6.07	s	20.19	40.39
0.4137	4.93	5.03	b	16.60	33.17
0.4137	5.49	5.51	s	18.33	36.68
0.3448	4.52	4.55	b	15.11	30.23
0.3448	4.84	4.85	s	16.15	32.31
0.2758	3.21	3.22	b	10.71	21.44
0.2758	3.80	3.82	s	12.71	25.40
0.2069	2.37	2.39	b	7.94	15.90
0.2069	2.95	2.96	s	9.851	9.71
0.1379	1.54	1.55	b	5.15	10.31
0.1379	2.03	2.03	s	6.76	13.51
0.1034	0.91	0.91	b	3.05	6.10
0.1034	1.42	1.42	s	4.74	9.50

\*wfp = wire feed pressure; avecm/s = average cm/sec used for each wire; tavecm/s = total average cm/sec of wire consumed during spraying.

\*\*b = bent; s = straight.

## Copper

### *Deposition Parameters*

Copper was sprayed at 25 V, 160 amps, a wire feed pressure of 6.1379 MPa psi, and a spray pressure of 0.4482 MPa psi with air as the spraying gas. For copper wire, there appeared to be a maximum wire feed rate; spraying above this rate caused the arc to be discontinuous due to sliding contact between the wires. The power cables to the sprayer were observed to jerk often as the arc was established and extinguished, indicating that the peak values of current existing during spraying were in excess of the 160 amps read on the meter.

Difficulty was experienced with spraying short, fixed lengths of wire; this problem resulted in short lengths of wire being burned off without being melted. To spray a controlled length, the wire was marked with respect to a fixed reference point on the sprayer. The wire was then wound back onto the bulk spool before spraying. An assistant was required during spraying to shut down the sprayer when the mark reached the reference point. This procedure made it possible to spray a fixed length of material.

Burned holes in the paper substrates at short spray distances (15 and 30 cm) also were a problem. Spraying onto aluminum foil at 15 cm created a hole about 1.25 cm in diameter near the spray center and numerous smaller penetrations from large droplets in the surrounding deposit. Spraying onto aluminum foil at 46 cm produced numerous small penetrations throughout the deposit. Spraying onto brick deposited a reasonably adherent coating on the unprepared surface. In one small region, the coating spalled and the curvature of the remaining coating surrounding this region indicated residual tensile stress in the coating. Several bumps up to about 0.3 cm diameter were visible on the brick surface indicating incomplete melting of the wire during spraying. Due to these problems, opacity thickness was not determined for this material. In addition, no bend tests were conducted.

### *Deposited Mass*

The deposited mass in grams for coatings sprayed onto graph paper was determined and is shown below. The low deposited mass at 15 and 30 cm occurred because holes were burned in the paper at these spray distances. Copper appeared to adhere well to the foil substrates; however, there was penetration of the foil by droplets even at large spray distances (18 cm).

Spray distance (cm)	15	30	46	61	76
Deposited mass (g)	0.95	2.12	3.19	1.37	0.27

### *Deposit Efficiency*

The deposit efficiency was calculated using a value of 34.66 g for the sprayed mass. The results appear below. From these data, it can be seen that the deposit efficiency of copper onto graph paper is poor.

Spray distance (cm)	15	30	46	61	76
Deposit efficiency	0.03	0.06	0.11	0.04	0.01

### *Radius of Conductivity*

The ROC for arc-sprayed copper was determined for each of the spray distances as listed below. Even though holes were burned through the substrates, values were measurable at short spray distances because a continuous conductive film had formed around the holes.

Spray distance (cm)	15	30	46	61	76
ROC (cm)	2.8	3.2	3.7	0.6	0.0

### *Radius of Opacity*

None of the coatings sprayed onto paper were completely opaque. The coatings sprayed at 15 and 30 cm had large holes due to burning away of the substrate. The coating sprayed at 46 cm had pinholes and a hole about 0.3 by 0.4 cm, possibly created by a projected piece of partially melted wire. Pinholes were also observed in copper sprayed onto aluminum foil. The material sprayed onto a brick appeared fully opaque; however, it was not possible to verify this by light transmission.

### *SEM Observations*

Fracture of coatings sprayed onto brick and aluminum foil indicated that failure was largely by delamination between individual particles which occurred without extensive plastic deformation.

### *Wire Feed Rate Measurements*

The wire feed rate was measured (Table 3). These data show that, in the pressure range used for spraying (wfp = 0.1379 MPa), there was a difference of about a factor of 3 in the wire feed rate for the bent and straight conditions. That explains the difficulty encountered in optimizing the spraying conditions. It probably would have been better to spray copper using a higher capacity power supply that could handle the large transient currents during actual arcing so that a higher wire feed pressure could be used, making operation less sensitive to wire feed tube bending. Another alternative would be to modify the wire feed mechanism to ensure a constant wire feed rate, regardless of the wire feed tube bending.

### *Maximum Droplet Temperature Calculation*

For the typical copper spraying parameters of 25 V, 160 amps, and 0.1379 MPa wire feed pressure (about 8.12 cm/sec), there are about 42.255 kcal of heat available for each mole of material being sprayed. It takes 7.037 kcal to heat 1 mole of copper from room temperature to its melting point and 3.11 kcal to melt 1 mole of copper at 1356 K. It takes 0.339 kcal to heat the molten copper from 1356 K to its boiling point at 2868 K. So far, this accounts for 14.456 kcal of the available energy; the rest is used to create vapor at 72.8 kcal/mole of vapor at 2868 K which results in 0.38 moles of vapor and 0.62 moles of liquid at 2868 K. In actual practice, the radiation and thermal conduction to the surroundings would be very significant at the temperatures of molten copper, so that boiling of the material probably would not be observed.

### *Maximum Stable Droplet Size Calculation*

The maximum stable droplet size for copper was calculated for several spray pressures by assuming a surface tension value of 1350 dynes/cm. At 0.1034 MPa,  $r$  was  $2.61 \times 10^{-3}$  cm. At 0.4137 MPa,  $r$  was  $2.61 \times 10^{-4}$  cm. At 0.6206 MPa,  $r$  was  $4.35 \times 10^{-4}$  cm. The value for surface tension was taken from the *CRC Handbook of Chemistry and Physics*.

### *Consumption Calculations*

The energy consumption was calculated to be about 24.88 kJ/cm<sup>3</sup> (6.91 W-hr/cm<sup>3</sup>). The material cost 6.29/kg which is about \$0.0561/cm<sup>3</sup>.

**Table 3**  
**Wire Feed Rate Measurements for Copper\***

wfp (MPa)	Left (m)	Right (m)	Hose**	avecm/s	tavecm/s
0.6206	5.68	6.23	b	19.66	39.32
0.6206	6.63	6.68	s	22.18	44.35
0.5516	5.35	5.62	b	18.28	36.58
0.5516	6.18	6.23	s	20.69	41.40
0.4827	4.88	5.11	b	16.67	33.27
0.4827	5.73	5.78	s	19.18	38.35
0.4137	4.19	4.48	b	14.48	28.91
0.4137	5.27	5.31	s	17.63	35.26
0.3448	3.49	3.70	b	11.98	23.98
0.3448	4.56	4.60	s	15.26	30.53
0.2758	2.57	2.73	b	8.83	17.68
0.2758	3.78	3.84	s	12.70	25.40
0.2069	1.77	1.85	b	6.04	12.09
0.2069	2.81	2.84	s	9.41	18.80
0.1379	0.47	0.51	b	1.63	3.25
0.1379	1.65	1.67	s	5.54	11.07
0.1034	0	0	b	0	0
0.1034	0.93	0.95	s	3.13	6.25

\* wfp = wire feed pressure; avecm/sec = average cm/sec used for each wire;  
tavecm/sec = total average cm/sec of wire consumed during spraying.

\*\* b = bent; s = straight.

## Iron (Low-Carbon Steel)

Bend testing, ROC, radius of opacity, and opacity thickness were not performed for this material.

### *Deposition Parameters*

Low-carbon steel was sprayed at 25 V, 200 amps, a wire feed pressure of 0.3448 MPa, and a spray pressure of 0.4137 MPa with air as the spraying gas (AS17). This material was sprayed onto both graph paper and brick substrates. Burning of the graph paper at a 15-cm spray distance was observed and very little of the mass of material sprayed was deposited onto the substrates at large spray distances; it appeared that much of the iron was burned by the air jet before it could be deposited at large spray distances.

Material sprayed at low thicknesses onto brick appeared to be very adherent; material sprayed at high thicknesses delaminated in a manner indicating strong residual tensile stress in the coating. The delaminated material had large amounts of the substrate (brick) material embedded in its back surface. Substrate failure due to thermal shock during spraying was evident at the corners and edges of the brick; it would be reasonable to assume that thermal stress played a significant role in the substrate failure associated with delamination of the thick deposits. Burning of the deposited coating was observed for short spraying distances. This burning appeared to be promoted by the air jet and the coating structure. The material deposited on the brick had a dark bluish-gray appearance. Red rusting at fingerprints was evident after 4 months' exposure to an office environment.

### *Deposited Mass*

The deposited mass was measured and the results were:

Spray distance (cm)	15	30	46	6176
Deposited mass (g)	0.0	0.18	0.0	--

### *Deposit Efficiency*

The deposit efficiency for low-carbon steel was calculated using a value of 27.36 g for the sprayed mass (see results below). These data show that the deposition efficiency for low-carbon steel was very low. The use of an inert spraying gas may have improved this situation by reducing the metal's tendency to be oxidized by the propelling gas.

Spray distance (cm)	15	30	46	6176
Deposit efficiency	0.0	0.01	0.0	--

### *Radius of Conductivity*

The ROC was not measured because the coatings deposited onto the graph paper substrates were not electrically continuous. Ohmmeter probes of the material sprayed onto brick indicated that the coating was electrically conductive; however, the contacting resistance was high--on the order of 0.3 to 0.4 ohms for the low-carbon steel coating compared with 0.0 to 0.1 ohms for zinc coatings. From this result, it appears that low-carbon steel coatings sprayed in this way would not be suitable for applications requiring electrical continuity through mechanical contacting of the sprayed surfaces.

### *Radius of Opacity*

The radius of opacity was not measured. Thick portions of coating that spalled off the brick substrate were observed to have pinhole porosity.

### *Opacity Thickness*

Opacity thickness was not observed for iron sprayed onto graph paper; however, measurements of the material sprayed onto brick indicated that it must be about 30  $\mu\text{m}$  (microns) or more.

### *SEM Observations*

SEM observations were made on a piece of the material sprayed onto the brick surface. Significant observations include:

1. There was a very fine structure in the back surface not seen in the front surface which was possibly due to contact with the brick surface; however, it was not noted on the back surface of other materials that were sprayed on brick and observed.
2. The coating appeared to fracture by delamination between particles and by brittle fracture of some particles with very little evidence of plastic deformation. Particle fracture must have occurred somewhat explosively (similar to bending a piece of plastic until it shatters into several pieces) since small fragments of material were observed on the fracture surface.
3. There was some evidence of delamination between individual layers during deformation and fracture.
4. Low-magnification inspection of the back surface indicated good conformation of the coating to the substrate surface topography.
5. Even though the low-carbon steel is heavily oxidized during spraying with air, there does not appear to be much of a problem with charge buildup on the surface during SEM observation.

### *Wire Feed Rate Measurements*

Wire feed rate was measured for the low-carbon steel wire. The results are listed in Table 4.

### *Maximum Droplet Temperature Calculation*

In addition to the assumptions described in Chapter 2, for the low-carbon steel wire, it was assumed that the carbon content is so low that the material can be treated as the thermodynamic equivalent of pure iron. For the typical iron spraying parameters of 25 V, 200 amps, and 0.3448 MPa wire feed pressure (about 31.50 cm/sec total), there is about 13.61 kcal of heat available for each mole of material being sprayed. It takes 6.053 kcal to heat 1 mole of iron from room temperature to the 1033 K alpha-to-beta transition temperature and 0.410 kcal to transform it to beta. Another 1.529 kcal is needed to heat 1 mole of beta iron to the 1180 K beta-to-gamma transition temperature and 0.217 kcal to transform it to gamma. It takes 4.501 kcal to heat 1 mole of gamma iron to the 1673 K gamma-to-delta transition temperature and 0.150 kcal to make the transition. So far, this process has used 12.86 kcal, leaving 0.75 kcal available for further heating. Heating 1 mole of delta iron to the 1808 K melting point requires 1.390 kcal and melting requires 3.860 kcal/mole. The remaining heat

Table 4

## Wire Feed Rate Measurements for Iron (Low-Carbon Steel)\*

wfp (MPa)	Left (m)	Right (m)	Hose**	avecm/s	tavecm/s
0.6206	6.31	6.37	b	21.13	42.27
0.6206	6.87	6.88	s	22.93	45.87
0.5516	6.15	6.20	b	20.57	41.15
0.5516	6.48	6.48	s	21.59	43.18
0.4827	5.73	5.77	b	19.16	38.30
0.4827	6.07	6.07	s	20.23	40.49
0.4137	5.25	5.28	b	17.55	35.10
0.4137	5.52	5.54	s	18.42	36.88
0.3448	4.64	4.65	b	15.49	30.99
0.3448	4.91	4.91	s	16.38	32.77
0.2758	3.94	3.96	b	13.17	26.31
0.2758	4.15	4.15	s	13.83	27.69
0.2069	3.06	3.09	b	10.25	20.47
0.2069	3.38	3.38	s	11.26	22.50
0.1379	1.97	1.98	b	6.58	13.16
0.1379	2.32	2.32	s	7.73	15.44
0.1034	1.40	1.40	b	4.66	9.30
0.1034	1.66	1.66	s	5.55	11.07
0.0690	0.30	0	b	0	0
0.0690	1.05	1.05	s	3.53	7.01

\*wfp = wire feed pressure; avecm/sec = average cm/sec for each wire;  
tavecm/s = total average cm/sec of wire consumed during spraying.

\*\*b = bent; s = straight.

available can only bring the material to 1746 K, which is below the melting point. For iron-carbon, the beginning of the melt zone can be depressed to 1746 K by adding about 0.3 weight percent carbon to the iron, which is pushing the upper limit for the carbon content of "low carbon steels." In truth, the melting temperature would have to be further depressed by larger additions of carbon to supply the energy for melting and to place the material far enough into the two-phase field to allow droplet formation, in addition to accounting for heat losses to the environment during spraying. Evidently, exothermic oxidation of the iron by the propelling air provides a major portion of the energy required for melting the metal as it is sprayed. This finding implies that, when arc-spraying low-carbon steel with air as the spray gas, the actual material being deposited is a mixture of iron and iron oxide.

#### *Maximum Stable Droplet Size Calculation*

The maximum stable droplet size for low-carbon steel was calculated for several spray pressure values by assuming a surface tension value of 1880 dynes/cm. At 0.1034 MPa,  $r$  was  $3.64 \times 10^{-3}$  cm. At 0.327 MPa,  $r$  was  $9.09 \times 10^{-3}$  cm. At 0.206 MPa,  $r$  was  $6.06 \times 10^{-3}$  cm. The value for surface tension used was that for pure iron taken from the *CRC Handbook of Chemistry and Physics*.

#### *Consumption Calculations*

The energy consumption was calculated to be about 8.0 kJ/cm<sup>2</sup> (2.23 W-hr/cm<sup>2</sup>). The material cost \$1.97/kg, which is \$0.0313/cm<sup>2</sup>.

### **13 Percent Chrome Steel (AS21)**

#### *Deposition Parameters*

The 13 percent chrome steel was sprayed at 25 V, 175 amps, a wire feed pressure of 0.2758 MPa, and a spray pressure of 0.4137 MPa with air as the spraying gas.

#### *Deposited Mass*

The deposited mass was not measured. The high temperatures associated with spraying this material caused the graph paper substrates to ignite even at a spray distance of 76 cm. Clearly, this material would not be suitable as a shielding material for direct spraying onto organic construction materials or inorganic materials coated with organics such as paint. For this reason, the following tests were not run: deposit efficiency, ROC, radius of opacity, opacity thickness, bend testing, and SEM observations.

#### *Wire Feed Rate Measurements*

The wire feed rate was measured for 13 percent chrome steel and results are presented in Table 5.

#### *Maximum Droplet Temperature Calculation*

No suitable thermodynamic data were located for doing this calculation.

#### *Maximum Stable Droplet Size Calculation*

The maximum stable droplet size was not calculated due to lack of availability of surface tension data available for the alloy.

**Table 5**  
**Wire Feed Rate Measurements for 13 Percent Chrome Steel**

wfp (MPa)	Left (m)	Right (m)	Hose**	avecm/s	tavecm/s
0.6206	5.67	5.93	b	19.33	38.66
0.6206	6.53	6.55	s	21.80	43.59
0.5516	5.70	5.80	b	19.18	38.35
0.5516	6.08	6.10	s	20.30	40.59
0.4827	5.21	5.30	b	17.51	35.00
0.4827	5.77	5.78	s	19.25	38.51
0.4137	4.85	4.90	b	16.26	32.51
0.4137	5.30	5.32	s	17.70	35.41
0.3448	4.26	4.31	b	14.29	28.60
0.3448	4.76	4.78	s	15.89	31.75
0.2758	3.76	3.80	b	12.60	25.20
0.2758	4.11	4.13	s	13.74	27.58
0.2069	2.87	2.90	b	9.61	19.20
0.2069	3.34	3.35	s	11.15	22.30
0.1379	1.84	1.85	b	6.14	12.29
0.1379	2.19	2.20	s	7.32	14.63
0.1034	1.11	1.12	b	3.72	7.47
0.1034	1.52	1.52	s	5.08	10.16
0.0690	0.08	0.08	b	0.25	0.51
0.0690	0.72	0.72	s	2.41	4.83

\* wfp = wire feed pressure; avecm/s = average cm/sec used for each wire;  
tavecm/s = total average cm/sec of wire consumed during spraying.

\*\* b = bent; s = straight.

### *Consumption Calculations*

The energy consumption was calculated to be about 8.4 kJ/cm<sup>3</sup> (2.33 W-hr/cm<sup>3</sup>). The material cost \$7.83/kg, which is about \$0.0615/cm<sup>3</sup>.

## **Nickel**

### *Deposition Parameters*

Nickel was sprayed at 25 V, 225 amps, a wire feed pressure of 0.3103 MPa, and a spray pressure of 0.4137 MPa with air as the spraying gas (AS23).

### *Deposited Mass*

The deposited mass was not measured. The high temperature of the depositing material burned holes through the paper substrates out to a distance of 61 cm. An aluminum foil substrate sprayed at 46 cm had a hole approximately 6.4 cm by 8.9 cm burned in the spray center and several smaller holes of at least 0.3 cm diameter burned in the surrounding foil. The smaller holes were probably made by incompletely melted pieces of wire projected from the sprayer. Apparently, this material would not be suitable for spraying on organic construction materials. Therefore, the following properties were not observed: deposit efficiency, radius of conductivity, radius of opacity, opacity thickness, bend testing, and SEM observations.

### *Wire Feed Rate Measurements*

The wire feed rate was measured for nickel wire and results are shown in Table 6. The data show that wire feeding for nickel followed the same trends observed for the other wires. At an operating pressure of 0.3103 MPa, there was about a 20 percent difference between the bent and straight conditions in wire feed rate.

### *Maximum Droplet Temperature Calculation*

For the typical nickel spraying parameters of 25 V, 225 amps, and 0.3103 MPa wire feed pressure (about 25.4 cm/sec total), there were about 17.65 kcal of heat available for each mole of material being sprayed. It takes 2.398 kcal to heat 1 mole of nickel from room temperature to the 626 K alpha-to-beta transition temperature and 0.092 kcal to transform it to beta. Another 8.947 kcal are needed to heat the beta nickel to the 1728 K melting point, plus 4.21 kcal to melt the nickel. So far, 15.647 kcal have been used and the remaining 1.978 kcal are available to heat the melted nickel to 1945 K. The high temperature and high melting point of nickel account for the substrate burning observed.

### *Maximum Stable Droplet Size Calculation*

The maximum stable droplet size for nickel was calculated for several spray pressure values by assuming a surface tension value of 1770 dynes/cm. At 0.1034 MPa,  $r$  was  $3.43 \times 10^{-3}$  cm. At 0.4137 MPa,  $r$  was  $8.56 \times 10^{-4}$  cm. At 0.6206 MPa,  $r$  was  $5.70 \times 10^{-4}$  cm.

### *Consumption Calculations*

The energy consumption was calculated to be about 11.2 kJ/cm<sup>3</sup> (3.11 W-hr/cm<sup>3</sup>). The material cost \$24.16/kg, or about \$0.2149/cm<sup>3</sup>.

**Table 6**  
**Wire Feed Rate Measurements for Nickel\***

wfp (MPa)	Left (m)	Right (m)	Hose**	avecm/s	tavecm/s
0.6206	5.26	5.33	b	17.65	35.31
0.6206	6.31	6.31	s	21.04	42.06
0.5516	5.03	5.09	b	16.86	33.73
0.5516	6.06	6.06	s	20.19	40.39
0.4827	4.80	4.81	b	16.02	32.05
0.4827	5.64	5.64	s	18.80	37.59
0.4137	4.33	4.36	b	14.48	28.96
0.4137	5.10	5.11	s	17.02	34.04
0.3448	3.75	3.77	b	12.53	25.04
0.3448	4.52	4.52	s	15.07	30.12
0.2758	3.01	3.04	b	10.07	20.17
0.2758	3.85	3.86	s	12.85	25.70
0.2069	2.11	2.12	b	7.05	14.12
0.2069	2.90	1.08	s	9.67	19.35
0.1379	1.08	1.08	b	3.60	7.21
0.1379	1.78	1.78	s	5.93	11.84
0.1034	0.32	0.32	b	1.06	2.13
0.1034	1.12	1.12	s	3.72	7.47
0.0690	0	0	b	0	0
0.690	0.127	0.13	s	0.42	0.86

\*wfp = wire feed pressure; avecm/s = average cm/sec used for each wire;  
tavecm/s = total average cm/sec of wire consumed during spraying.

\*\*b = bent; s = straight.

## Nickel-Chrome

### *Deposition Parameters*

The nickel-chromium alloy was sprayed at 25 V, 230 amps, a wire feed pressure of 0.3448 MPa, and a spray pressure of 0.4137 MPa. Holes were burned through the graph paper substrates at spray distances up to 76 cm. A large hole some 8.9 cm in diameter was burned in the aluminum foil substrate at 46 cm. There were many smaller holes of about 0.1 to 0.3 cm diameter in the region surrounding the large hole. Apparently, the high deposition temperature of this material makes it unsuitable for coating organic materials. Therefore, the following tests were not performed: deposited mass, deposit efficiency, ROC, radius of opacity, opacity thickness, bend testing, and SEM observations.

### *Wire Feed Rate Measurements*

Wire feed rate was measured for the nickel-chromium alloy. Table 7 reports the data.

### *Maximum Droplet Temperature Calculation*

No suitable thermodynamic data were located to do the calculation on this alloy.

### *Maximum Stable Droplet Size Calculation*

The maximum stable droplet size was not calculated because surface tension data for this alloy are not available. The nickel-chrome droplets deposited on the surface of the aluminum foil appear to be slightly larger than those in the nickel test.

### *Consumption Calculations*

The energy consumption was calculated to be about 11.5 kJ/cm<sup>3</sup> (3.19 W-hr/cm<sup>3</sup>). The material cost \$21.72/kg, which is about \$0.1705/cm<sup>3</sup>.

## Tin

Opacity thickness was not measured for tin. In addition, bend testing was not conducted.

### *Deposition Parameters*

Tin was sprayed at 25 V, 75 amps, a wire feed pressure of 0.5516 MPa, and a spray pressure of 0.4137 MPa with air as the spraying gas (AS18). The wire used for tin spraying was available only in 0.1981-cm size as opposed to the 0.1588-cm-diameter wires used for spraying all the other metals. Spraying tin produced a cloud of yellow smoke which was much more irritating to the operator than the fumes associated with spraying other materials such as zinc. Spraying at large distances tended to produce a deposit having a yellowish color. Also, tin wire is almost too soft to handle. The feeding problems were more frequent than with any other metal sprayed. Problems included: (1) wire breaking between the spools and wire drivers caused by the resistance to supply spools' turning and (2) pileup of the wire in front of the wire drivers due to debris in the sprayer tips. However, the wire was easy to remove from the tips--unlike the case for which zinc pileups occur, because the zinc wire fuses to the sprayer tips.

Table 7  
Wire Feed Rate for Nickel-Chromium Alloy\*

wfp (MPa)	Left (m)	Right (m)	Hose**	avecm/s	tavecm/s
0.6206	4.78	4.78	b	15.93	31.85
0.6206	6.23	6.25	s	20.80	41.61
0.5516	4.38	4.45	b	14.71	29.41
0.5516	5.66	5.68	s	18.90	37.80
0.4827	3.95	3.99	b	13.24	26.47
0.4827	5.30	5.30	s	17.66	35.31
0.4137	3.35	3.38	b	11.22	22.45
0.4137	4.80	4.81	s	16.01	32.06
0.3448	3.07	3.23	b	10.49	20.98
0.3448	4.24	4.24	s	14.12	28.24
0.2758	2.44	2.60	b	8.40	16.81
0.2758	3.70	3.73	s	12.39	24.79
0.2069	1.79	1.86	b	6.09	12.19
0.2069	2.88	2.90	s	9.63	19.25
0.1379	1.00	1.02	b	3.38	6.76
0.1379	1.64	1.64	s	5.47	10.92
0.1034	0	0	b	0	0
0.1034	1.04	1.04	s	3.46	6.91
0.0690	0	0	b	0	0
0.0690	0.56	0.56	s	1.86	3.71

\*wfp = wire feed pressure; avecm/s = average cm/sec used for each wire;  
tavecm/s = total average cm/sec of wire consumed during spraying.

\*\*b = bent; s = straight.

### *Deposited Mass*

The deposited mass in grams for coatings sprayed onto graph paper was determined. A low value occurred at 15 cm because a hole was burned through the middle of the substrate and the area of paper and tin was lost. Deposited mass results for tin (AS18) were:

Spray distance (cm)	15	30	46	61	76
Deposited mass (g)	5.05	14.2	6.89	3.44	0.93

### *Deposit Efficiency*

The deposit efficiency was calculated using a value of 37.36 g for the sprayed mass. The results were:

Spray distance (cm)	15	30	46	61	76
Deposit efficiency	0.14	0.38	0.19	0.09	0.02

### *Radius of Conductivity*

The ROC was determined for each spray distance. Values were:

Spray distance (cm)	15	30	46	61	76
ROC (cm)	5.41	5.92	5.64	5.46	3.51

### *Radius of Opacity*

The radius of opacity was not measured. All coatings sprayed at 30 cm or farther had pinhole porosity throughout. The coating sprayed at 15 cm burned a large hole in the spray center of the substrate.

### *SEM Observations*

No SEM observations were attempted; however, visual observations were made. Significant among these observations were: (1) the bubbly central regions present only at 6 in. for the zinc coatings (see the next section) persisted to a distance of 61 cm with the tin coatings; this result is probably strongly related to the lower melting point of tin, (2) at a spray distance of 15 cm, the molten layer built sufficient thickness on the substrate to be blown out of the center by the laterally deflected air stream; this finding supports the possibility for radial motion of depositing particles at the substrate surface under the influence of a "lateral breeze" (Figure 1).

### *Wire Feed Rate Measurements*

Wire feed rate measurements were abandoned due to difficulties with feeding the wire. With tin, having the feed tubes straight rather than bent made the difference between the wire feeding or breaking. In the case of 0.6206 MPa wire feed pressure with the feed tubes bent, the wire in the left tube broke at the start and the right wire fed 5.50 m within 30 sec.

### Maximum Droplet Temperature Calculation

For the typical tin spraying parameters of 25 V, 75 amps, and 0.5516 MPa of wire feed pressure (about 40.64 cm/sec total), there were about 5.715 kcal of heat available for each mole of material being sprayed. It takes 1.439 kcal to heat 1 mole of tin from room temperature to the 505 K melting point and 1.690 kcal to melt it. This process leaves 2.586 kcal that heat the liquid to 859 K.

### Maximum Stable Droplet Size Calculation

The maximum stable droplet size for tin was calculated for several spray pressure values by assuming a surface tension value of 560 dynes/cm. At 0.1034 MPa,  $r$  was  $1.08 \times 10^{-3}$  cm. At 0.4137 MPa,  $r$  was  $2.71 \times 10^{-4}$  cm, and at 0.6206 MPa,  $r$  was  $1.80 \times 10^{-4}$  cm. The value for surface tension is that for pure tin from the *CRC Handbook of Chemistry and Physics*.

### Consumption Calculations

The energy consumption was calculated to be about 1.47 kJ/cm<sup>3</sup> (0.41 W-hr/cm<sup>3</sup>). The material cost \$32.52/kg, or \$0.2368/cm<sup>3</sup>.

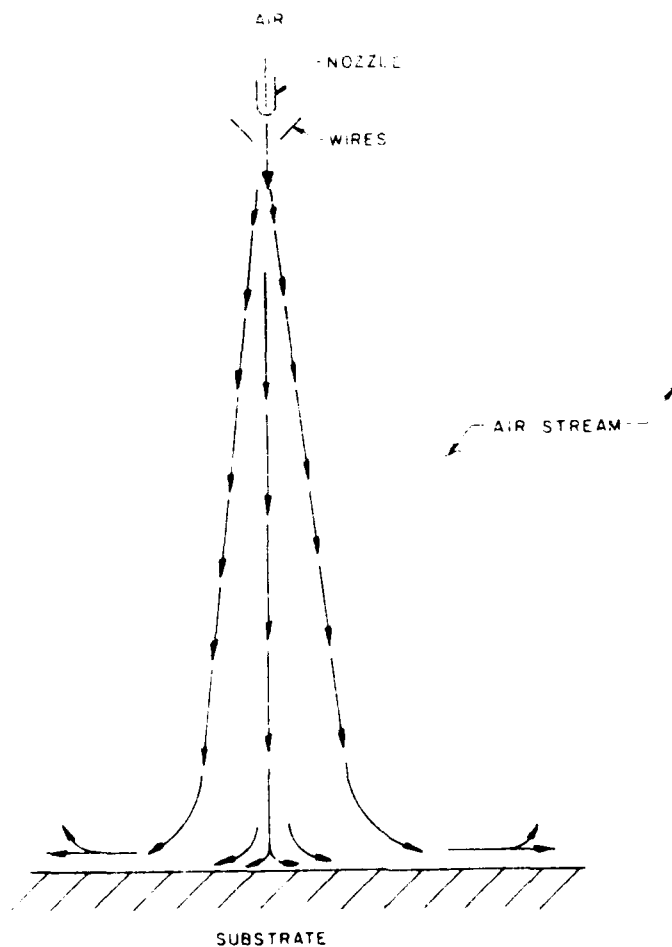


Figure 1. "Lateral breeze" generation which gives rise to droplet motion parallel to the substrate surfaces at locations away from the spray center.

## Zinc

### *Deposition Parameters*

A wide range of deposition parameters was used for spraying zinc because it is the metal which is arc-sprayed most often. The data from sprayed zinc was analyzed to observe trends that could be used to minimize the time required to find the optimal spraying parameters for the other materials sprayed. Table 8 lists the deposition parameters for testing this material. Wire lengths indicated with a "t" such as t15 or t4, are actually approximate spraying times in seconds. The "times" were monitored by lightning counts (one thousand one, one thousand two, etc.) so the absolute value of the data from these coatings has significant error; however, the general trends should be valid. Coatings done by timing were spool-fed so that the actual current during spraying may have differed from that registered during the setup due to the effects that bending the wire feed tubes had on the wire feed rate. Coatings formed using cut lengths of wire used the wire feed spools; therefore, the actual wire feed rate and current during spraying were higher than the values listed in the table.

### *Deposited Mass*

The deposited mass in grams was determined for coatings sprayed onto graph paper (Table 9). The N2 value for 46 cm is the average of six samples. The AIR value for 46 cm is the average of five samples.

The effects of zinc spraying conditions on deposited mass are summarized below.

1. Deposited mass decreased with increasing spray distance. A reasonable explanation for this observation is that some particles solidify in flight while traveling the source-to-substrate distance and are reflected from the substrate. The probability of the particle cooling before impact increases with increasing source-to-substrate distance. Smaller particles should cool first since their surface area-to-volume ratio is greater than that of a larger particle.

2. Deposited mass increased with increasing spray time.

3. Decreasing the arc voltage during spraying tended to decrease the deposited mass, especially at long distances. A reasonable explanation for this is that, at reduced voltage (and hence reduced current and total power), superheating of the molten droplets by the arc is reduced and, therefore, the probability that they will solidify in flight and be reflected from the substrate increases. Another explanation is that, at high power and the same gas flow rate, the spray gas can be heated to a higher temperature, thus reducing the cooling rate of the droplets being conveyed by it.

4. Reducing spraying pressure tended to increase deposit mass at large spraying distances. A reasonable explanation for this finding is that, at a given temperature, a molten metal has a specific surface tension. The spraying pressure must work to overcome this surface tension in forming a droplet from the molten metal. A higher spraying pressure can form a smaller droplet while a lower spraying pressure requires that a larger droplet be formed before it can be pulled from the melt. This condition indicates that the average droplet size will increase with decreasing spray pressure and, since a larger droplet is more likely to remain molten and adhere to the substrate at longer spraying distances, the deposited mass at large spraying distances should increase with decreasing spraying pressure. Reducing spray pressure also reduces the volume of gas to be heated by the arc.

5. Increasing wire feed rate increased the deposited mass at short spraying distances. A possible explanation for this finding is that, at higher wire feed rates, the heat of the arc must penetrate more material to be melted; this results in less superheating of the melt. The lower melt temperature

Table 8  
Spraying Parameters for Zinc Tests

Zinc Condition	Volts	Amps	wfp* (MPa)	Spray (Mpa)	Wire Length (cm)	Gas
AS1	21	100	0.4137	0.6068	t15	air
AS2	21	100	0.4137	0.6068	t4	air
AS3-2	21	100	0.4137	0.6068	t2	air
AS3-4	21	100	0.4137	0.6068	t4	air
AS3-8	21	100	0.4137	0.6068	t8	air
AS3-16	21	100	0.4137	0.6068	t16	air
AS4-2	17	100	0.4137	0.4482	t2	air
AS4-4	17	100	0.4137	0.4482	t4	air
AS4-8	17	100	0.4137	0.4482	t8	air
AS4-16	17	100	0.4137	0.4482	t16	air
AS5-2	23	140	0.4137	0.6068	t2	air
AS5-4	23	140	0.4137	0.6068	t4	air
AS5-8	23	140	0.4137	0.6068	t8	air
AS5-16	23	140	0.4137	0.6068	t16	air
AS6-2	20	135	0.5516	0.6206	t2	air
AS6-4	20	135	0.5516	0.6206	t4	air
AS6-8	20	135	0.5516	0.6206	t8	air
AS6-16	20	135	0.5516	0.6206	t16	air
	17	100	0.4137	0.4482		air
	20	130	0.4137	0.4482		air
	23	140	0.4137	0.4482		air
	25	150	0.4137	0.4482		air
	25	145	0.4137	0.4827		air
	23	140	0.4137	0.4827		air
	20	130	0.4137	0.4827		air

Table 8 (Cont'd)

Zinc Condition	Volts	Amps	wfp* (MPa)	Spray (Mpa)	Wire Length (cm)	Gas
AS6-16	20	125	0.4137	0.5516		air
(cont'd)	23	145	0.4137	0.5516		air
	25	150	0.4137	0.5516		air
	18	100	0.4137	0.5516		air
AS7	25	200	0.5516	0.6206	15	air
AS7-B	25	200	0.5516	0.4137	15	air
AS8	20	175	0.5516	0.6206	15	air
AS8-B	20	175	0.5516	0.4137	15	air
AS9	25	150	0.4137	0.6206	15	air
AS9-B	25	150	0.4137	0.4137	15	air
AS10	25	160	0.4137	0.6206	106.7	air
AS11	25	200	0.5516	0.6206	106.7	air
AS12	25	180	0.4137	0.4137	106.7	air
AS13	18	120	0.4137	0.6206	106.7	air
AS14	25	175	0.5516	0.4137	106.7	air
AS15	25	210	0.5516	0.6206	45.7	air
N2	25	180	0.5516	0.4137	106.7	nitrogen
AIR	25	180	0.5516	0.4137	106.7	nitrogen

\*Wire feed pressure.

increases viscosity and surface tension; thus, the droplet size for a given spray pressure will increase, but the droplet temperature will be lowered. Larger droplets will cover a greater area on the substrate upon impact and thus have a greater chance of coating a binding site and adhering to the substrate. The lower droplet temperature implies that solidification may occur more rapidly over a shorter spray distance, with reduced adherence at larger spray distances. The effect of reducing spray pressure is more pronounced than that of increasing wire feed rate at large spray distances.

#### *Deposit Efficiency*

The deposit efficiency was calculated using a value of 25.5 g for the sprayed mass of 106.7 cm wire lengths and a value of 7.67 g for the sprayed mass of 46 cm wire lengths. The results are given in Table 10.

Table 9  
Deposited Mass (g) for Zinc Coatings  
Sprayed Onto Graph Paper

Zinc Condition	Spray Distance (cm)					
	15	30	46	61	76	91
AS3-2	4.00	1.90	1.06	0.78	0.47	
AS3-4	8.56	5.66	3.16	1.92	1.34	
AS3-8	17.9	9.95	8.43	5.00	2.83	
AS3-16	36.7	29.3	15.8	9.85	6.75	
AS4-2	4.15	3.27	1.81	0.90	0.40	
AS4-4	8.41	5.74	3.65	2.18	1.01	
AS4-8	17.5	12.9	7.29	3.97	2.34	
AS4-16	35.4	30.0	18.5	11.6	6.87	3.00
AS5-2	3.22	2.74	1.61	0.74	0.57	
AS5-4	7.10	5.52	2.98	1.79	1.04	
AS5-8	14.4	10.3	6.48	4.07	1.94	0.98
AS5-16	32.3	20.6	12.5	7.18	3.41	1.84
AS6-2	5.15	4.03	2.20	1.14	0.66	
AS6-4	10.8	6.94	3.74	2.70	1.44	0.75
AS6-8	24.6	15.5	10.2	5.49	3.69	2.15
AS6-16	53.3	33.1	24.2	14.4	8.86	5.17
AS10	14.0	8.95	6.35	4.19	2.39	1.35
AS11	16.6	9.90	6.79	3.96	2.27	1.28
AS12	14.9	8.64	6.78	5.26	2.45	2.13
AS13	13.5	8.82	3.54	1.53	0.59	
AS14	15.1	9.55	7.45	5.67	4.08	2.96
AS15	3.73	2.20	1.55	0.97	0.55	
N2	14.8	9.28	8.23	6.77	5.36	
AIR		6.31				

Table 9 (Cont'd)

	A	B	C	D	E	F	Avg	Std Dev
N <sub>2</sub> (x=46)	8.01	8.04	8.22	8.54	8.34	8.27	8.24	0.197
AIR(x=46)	6.44	6.09	6.41	6.23	6.40		6.31	0.150

The spraying conditions' effects on deposition efficiency are summarized below.

1. The deposit efficiency increased with increasing spray time. A possible explanation for this finding is that when deposition is just beginning, the substrate surface is relatively smooth such that it does not have projections onto which incoming droplets can lock and bond themselves to the surface. As deposition continues, the surface becomes roughened by deposited droplets that provide better bonding sites for the incoming droplets. This explanation suggests that the deposition rate is a function of surface roughness. The literature indicates that shotblasting the surface prior to deposition improves the adhesion of thermal-sprayed coatings by allowing more mechanical interlocking; the same treatment should also increase the deposition efficiency. Deposition efficiency should be strongly coupled to adhesion in the sense that the set of parameters producing a high deposition efficiency also cause the coating to adhere well to itself and the substrate.

2. Deposition efficiency decreased with increasing spray distance in parallel with the discussion under *Deposited Mass* above.

3. Decreasing the arc voltage during spraying tended to decrease the deposition efficiency; see the discussion under *Deposited Mass* above.

4. Reducing the spraying pressure increased deposition efficiency at large spraying distances as described above under *Deposited Mass*.

5. Similarly, increasing wire feed rate increased deposition efficiency at short spraying distances as described above.

6. Using nitrogen as the spraying gas improved the deposit efficiency, especially at larger spray distances (compare N<sub>2</sub>, AIR, and AS14).

7. There was a significant influence of surrounding temperature and spray gas temperature on the deposition efficiency. AS14 was sprayed in late June near midday and N<sub>2</sub> and AIR were sprayed near mid-November when it was very cold outside. The AIR coatings had a significantly lower deposit efficiency than the corresponding AS14 coating. Switching to nitrogen as spray gas compensated for the loss of deposition efficiency due to low temperatures--especially at longer spray distances.

Table 10  
Deposit Efficiency for Zinc Under Varied Spray Conditions

Zinc Condition	Spray Distance (cm)							
	15	30	46	61	76	91		
AS10	0.55	0.36	0.25	0.17	0.09	0.05		
AS11	0.66	0.39	0.27	0.16	0.09	0.05		
AS12	0.59	0.34	0.27	0.21	0.10	0.08		
AS13	0.53	0.35	0.14	0.06	0.02			
AS14	0.60	0.38	0.30	0.23	0.16	0.12		
AS15	0.49	0.29	0.20	0.13	0.07			
N2	0.59	0.37	0.33	0.27	0.21			
AIR		0.25						
	A	B	C	D	E	F	Avg	Std Dev
N2(x=46)	0.32	0.32	0.33	0.34	0.33	0.33	0.33	0.008
AIR(x=46)	0.26	0.24	0.25	0.25	0.25		0.25	0.006

#### *Radius of Conductivity*

The ROC was determined for each spray distance. Table 11 reports the findings.

The effect of spraying conditions on ROC had the following trends:

1. The ROC increased with increasing spraying time; this result implies that the ROC is proportional to the deposited mass, which also increased with increasing spraying time.
2. The ROC increased with increasing arc voltage, an occurrence probably coupled to the deposition efficiency which was low for a low arc voltage.

Table 11

## Radius of Conductivity (cm) for Zinc

Zinc Condition	Spray Distance (cm)					
	15	30	46	61	76	91
AS2	3.78	5.33	5.79	6.38	3.94	-
AS3-2	3.86	4.39	4.34	3.66	0	-
AS3-4	4.62	5.46	5.77	5.44	3.94	-
AS3-9	5.37	6.12	6.91	7.01	6.35	-
AS3-16	6.30	7.19	7.52	8.08	8.03	-
AS4-2	3.71	5.05	4.95	3.15	0	-
AS4-4	4.45	5.66	6.02	5.66	2.92	-
AS4-8	5.31	6.67	6.83	6.73	5.92	-
AS4-16	5.79	7.29	8.28	8.51	8.05	6.35
AS5-2	3.78	4.70	4.60	3.43	0	-
AS5-4	4.29	5.28	5.59	5.33	3.84	-
AS5-8	4.75	5.66	6.25	6.45	5.46	0
AS5-16	5.77	6.60	7.04	5.46	6.58	5.38
AS6-2	3.84	4.83	5.36	4.88	3.25	-
AS6-4	4.67	5.69	6.17	6.12	5.44	2.34
AS6-8	5.41	6.35	6.93	7.29	7.01	5.92
AS6-16	6.32	7.21	8.03	8.74	8.69	8.23
AS10	5.28	6.20	6.88	7.06	5.97	3.91
AS11	5.00	6.68	7.06	6.83	5.94	0
AS12	5.84	7.14	7.37	7.59	5.23	-
AS13	4.45	5.41	6.02	5.49	0	-
AS14	5.89	6.76	7.57	7.75	7.39	6.55

Table 11 (Cont'd)

Zinc Condition	Spray Distance (cm)						Avg	Std Dev
	15	30	46	61	76	91		
AS15	4.27	5.11	5.16	4.60	0	-		
N2	7.34	7.4	8.23	8.41	8.31	-		
AIR	-	-	7.24	-	-	-		
	A	B	C	D	E	F		
N <sub>2</sub> (x=46)	8.23	8.36	8.31	8.15	8.15	8.00	8.23	0.13
AIR (x=46)	7.44	7.14	7.26	6.99	7.37	-	7.24	0.18

3. There was an optimal spraying distance to maximize the ROC. This optimum represents a balance between the finite divergence of the spray stream and the decrease in deposit efficiency at large spray distances. At short spray distances, the deposition efficiency was high but the area covered by the spray stream was small, so the size of the conductive area formed was small. At large spray distances, the size of the area covered by the spray stream was large; however, the deposition efficiency was low and the impingement rate per unit area was small (impingement rate per unit area falls off roughly as one over distance squared), so the coating is deposited discontinuously over a large area, resulting in a small ROC. At intermediate spray distances, there is a balance between impingement rate, deposition efficiency, and area covered by the spray stream to give a maximum conductive area.

4. The optimal spraying distance increased with increasing spraying time.

5. An increase in the mass deposited should increase the size of the conductive area formed since the dose per unit area will increase.

6. The use of nitrogen as a spray gas was found to increase the size of the conductive area formed at all spray distances (compare N<sub>2</sub>, AIR, and AS14).

7. There is a temperature effect such that decreasing the temperature of the spray gas and the surroundings decreased the size of the conductive area formed.

#### *Radius of Opacity*

The radius of opacity was determined for zinc at each spray distance. Table 12 presents the findings.

**Table 12**  
**Radius of Opacity (cm) for Zinc**

Zinc Condition	Spray Distance (cm)					
	15	30	46	61	76	91
AS6-2	2.90	2.11	2.06	0	0	-
AS6-4	3.45	3.86	2.97	0.56	0	0
AS6-8	3.76	4.65	4.50	2.74	0	0
AS6-16	4.29	5.21	5.31	4.85	2.90	0
AS10	3.38	3.96	3.58	0	0	0
AS11	3.38	4.04	3.58	0	0	0
AS12	3.66	4.04	3.10	0	0	0
AS13	3.33	3.81	2.24	0	0	0
AS14	3.86	4.14	3.73	1.96	0	0
AS15	2.87	2.69	0	0	0	0
N2	3.89	3.81	3.45	0	0	-
AIR	-	3.48	-	-	-	-

	A	B	C	D	E	F	Avg	Std Dev
N2(x=46)	3.33	3.33	3.33	3.33	3.66	3.73	3.45	0.19
AIR(x=46)	3.51	3.51	3.58	3.56	3.30	-	3.48	0.11

The effects of spraying condition on radius of opacity are summarized below.

1. The radius of opacity increased with spraying time similar to the ROC.
2. There was an optimal spraying distance to maximize the radius of opacity; the reasoning is parallel to the situation for the ROC.
3. The optimal spraying distance increased with spraying time.

4. Reducing the spray pressure and increasing the wire feed rate increased the radius of opacity at all spraying distances. This result may be coupled to the improved spraying efficiency for these conditions.

5. Reducing the voltage reduced the radius of opacity at all spraying distances. This finding may be coupled to the poor deposit efficiency at these conditions.

6. The radius of opacity was always smaller than the radius of conductivity. This condition implies that the coating always became electrically continuous before it became opaque for the deposition conditions studied. For EMP/RFI applications, it suggests that an optically dense coating should provide adequate shielding as long as the coating thickness at the point of opacity is sufficiently larger than the skin depth of the frequency of interest.

7. At large spray distances, there were significant conductive areas while the coatings were completely porous.

8. Coatings sprayed with nitrogen appeared to have opaque areas similar in size to those sprayed with air; however, the nitrogen-sprayed coatings formed larger conductive areas. This result implies that oxide formation, which inhibits conductivity between particles at low coverage, is reduced by spraying with nitrogen.

#### *Opacity Thickness*

The opacity thickness was determined for zinc at each spray distance. Table 13 lists the results.

The opacity thickness increased with increasing spraying distance. This finding supports the idea that, as spray distance increases, only the larger particles that remain molten when they strike the substrate will adhere. For a rough approximation, as particle size increases, the interparticle pore size increases and thus the coating thickness required to produce an optically dense coating would increase. There was a significant effect of temperature on the opacity thickness; low temperatures of spraying gas and surroundings appeared to inhibit the deposition of smaller droplets by promoting freezing prior to impact, similar to the longer spray distances. Low temperatures probably also reduced the time available for droplet relaxation after impact before freezing, which gave rise to a rougher surface and an artificially higher thickness since the thickness probe rests on the peaks of surface roughness.

#### *Bend Testing*

Bend testing was conducted on zinc condition AS14 by spraying onto a smooth, thick aluminum sheet (about 0.32 cm). The zinc coating spalled off the smooth surface due to thermal stresses to provide freestanding sheets of coating for bend testing. Table 14 presents the results. A strain of 1.4 percent was assumed for the calculated breaking diameter.<sup>4</sup> The data indicate that the observed radii of curvature for coating rupture were less than the calculated values. A possible explanation is that coating thickness is measured from peak to peak of the coating surface roughness and the yielding of the coating is first accommodated in the thinnest regions of the coating which can be bent to a smaller radius before exceeding the critical strain for rupture. Before SEM observations were attempted, the

---

<sup>4</sup>Mathewson, C. H., *Zinc: The Science and Technology of the Metal, Its Alloys and Compounds* (Reinhold, 1959).

Table 13  
Opacity Thickness (microns) for Zinc

Zinc Condition	Spray Distance (cm)					
	15	30	46	61	76	91
AS10	84	99	119	-		
AS11	76	107	147	-		
AS12	69	109	150	-		
AS13	53	91	140	-		
Av(10-13)	71	102	140	-		
AS14	85	100	123	157		
AS15	44	67	-	-		
N2	124	147	150	-		
AIR	-	-	132	-		

	A	B	C	D	E	F	Avg	Std Dev
N2(x=46)	153	143	165	160	138	139	150	19
AIR(x=46)	135	132	130	144	118	-	132	13

graph paper and aluminum foil substrates were compared visually to assess the coatings. It was found that:

1. "Hail damage" type deformation occurred in the aluminum foil substrates in the region surrounding the coating for samples sprayed at large distances. This result indicates that a major portion of the coating flux is solidifying before reaching the substrate. Similar damage was not observed on the graph paper substrates; however, if it did occur, paper would not preserve the evidence as well as aluminum foil.

**Table 14**  
**Bend Test Results for Zinc (AS14)**

<b>Zinc Thickness (microns)</b>	<b>Observed Breaking Diameter (cm)*</b>	<b>Calculated Breaking Diameter (cm)</b>	<b>Opacity</b>
51	lt 0.32	0.36	Porous
64	lt 0.32	0.46	Porous
74	lt 0.32	0.53	Porous
76	lt 0.32	0.53	Porous
91	0.48	0.64	Opaque
122	0.48	0.86	Opaque
127	0.32	0.89	Opaque
137	0.32	0.97	Opaque
173	0.32	1.22	Opaque
178	0.48	1.24	Opaque
203	0.64	1.42	Opaque
229	0.64	1.60	Opaque
445	gt 2.5	3.12	Opaque
533	gt 1	3.73	Opaque

\*lt = less than; gt = greater than.

2. Delamination from the aluminum foil at large spray distances occurred in a roughly circular pattern around the spray center. The degree of partial delamination of individual particles was observed to be greater in directions away from the spray center than toward the center. A possible explanation for this finding is that as the particles approached the substrate surface, they were given a component of outward velocity by the air stream escaping from the spray center (refer to Figure 1). The outward motion would cause the droplets to flatten into an egg shape at impact on a flat, smooth surface. The more pointed end of the shape would be outward and the point of initial impact near the wider end

would be better bonded to the substrate. Another explanation for this observation in terms of the radial air stream across the surface is that if the deposited particles are sufficiently delaminated in the direction toward the spray center, the outward moving air stream can extend under the edge enough to cause complete delamination from the substrate, whereas the outwardly lifted edges would not be subject to this kind of stripping action.

3. The massive central region of the coatings sprayed at 15 cm almost completely delaminated from the substrate except at the very center, where the aluminum foil melted and the zinc penetrated it.

4. Coatings sprayed with nitrogen as the spray gas appeared slightly shinier than those sprayed with air, implying that perhaps the droplet surfaces oxidized less during flight. This explanation seems reasonable since thick, undeformable oxide skins are known to inhibit particle adhesion and the deposition efficiency of the nitrogen-sprayed coating (N<sub>2</sub>) was higher than that of the equivalent air-sprayed coating (AIR).

#### *SEM Observations*

Examination by SEM indicated that the coating structure was highly dependent on the spray distance and the distance from the spray center. The SEM micrographs were interpreted as described below.

Figure 2 is an SEM image of a typical zinc coating arc-sprayed at a distance of 15 cm. The structures observed mimic to some extent the processes giving rise to the structures observed in vacuum deposited coatings. The center region (A) is relatively smooth, indicating coating motion or flow after deposition. The region surrounding this area (B) shows a columnar type structure that indicates limited postdeposition motion and a tendency for shadowing effects.

Figure 3 is a highly magnified image of region A in Figure 2. In Figure 3a, the extensive presence of shrinkage marks similar to those observed in castings indicates that the droplets cooled and solidified well after impinging onto the surface. In Figure 3b, the crater-like features could possibly arise from the impact of the impinging particles or the escape of trapped gas bubbles. They may also be partly due to shadowing effects that were not completely smoothed out by droplet motion after impact. Or, they may be a result of the impinging air stream on the molten surface after deposition had ended.

Figure 4 is a highly magnified view of region B in Figure 2. Large intercolumnar voids are visible. The slight tapering of the columns (perhaps more visible in Figure 2) indicates some component of deposition flux in a direction radially outward from the spray center. Active self-shadowing mechanisms are present in both the radial direction from the spray center and the substrate normal direction. Note that the microscopic surface features in Figure 4 are smoother than those observed in Figure 3b.

Figure 5 is a high-magnification view of the column in Figure 4. There is an absence of shrinkage marks in this region, indicating that the cooling mode for the drops impacting the columns was different than that of drops impacting the spray center. Cooling in this region was probably similar to splat cooling coupled with spreading of the deposited droplets by the air blast. Note the relatively smooth surface (microscopic) compared with Figure 3a.

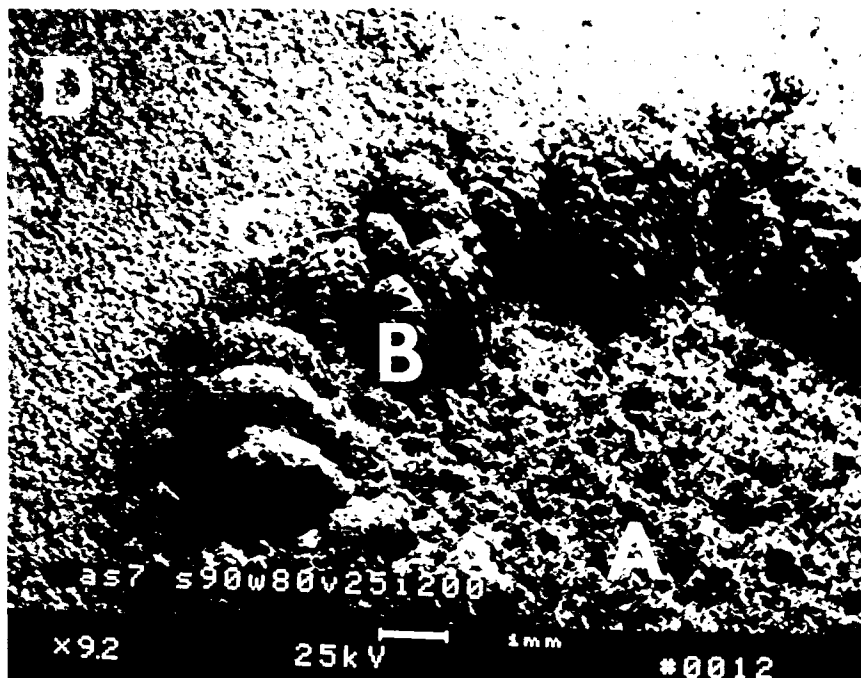


Figure 2. SEM micrograph of zinc arc-sprayed at a distance of 15 cm. The structure varies radially outward from the spray center.

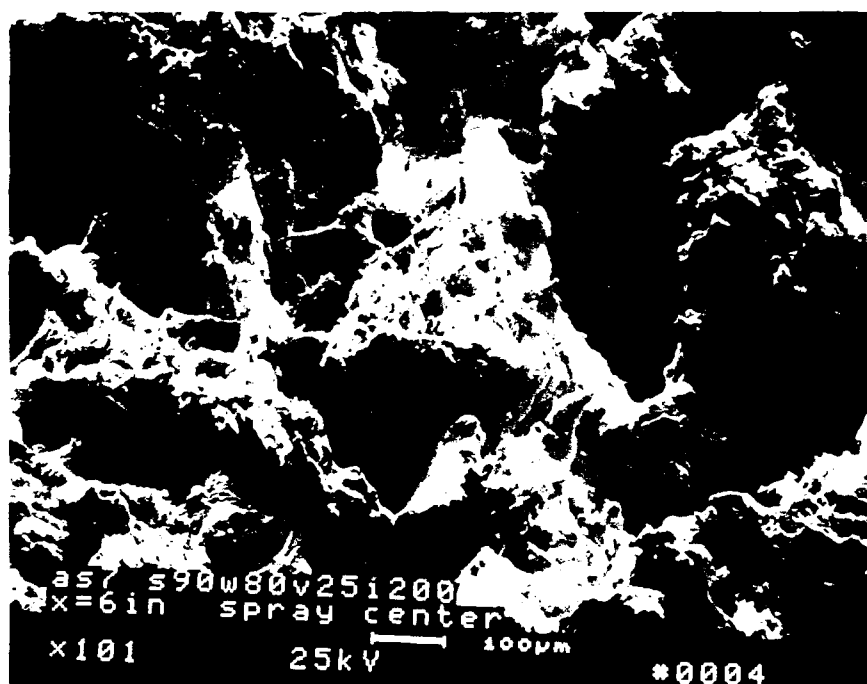
Figure 6 is a higher magnification view of region C in Figure 2. Note that the features in this region are finer than those observed in both Figures 3b and 4. The cooling mode in this region appears to be similar to that observed in region B of Figure 2. The deposition flux in this area is lower than in regions closer to the spray center; the influence of the radial substrate air stream would also be greater in this region as suggested in Figure 1.

Figure 7 is a more magnified view of Figure 6 showing the small, smooth regions for comparison to Figure 5. If the smooth regions arise from the spreading of droplets by the air blast after impact, then it seems reasonable that the smooth areas would be smaller farther away from the spray center since the substrate normal component of the air blast would decrease with radial distance from the spray center. Particles moving in a path away from the spray center would also be traveling slower before impact since the force acting to accelerate them is less than that for a particle traveling to the spray center.

Figure 8 is a highly magnified view of a region even farther from the spray center (approximately at location D on Figure 2). At this region, a further increase in surface roughness is observed. Droplet shape is approximately like that of a red blood cell which has been deformed to conform to the shape of the local substrate roughness. If deposited on a smooth surface, the droplets would be roughly egg-shaped in the substrate normal projection and thinner between the edges and middle than at those positions as shown in Figure 9. The shape arises from the combined effects of the droplet trajectory being nonnormal to the substrate, the radial air stream present at the substrate surface, and the tendency for the highest quench rate to be at the initial point of impact. Shrinkage marks are visible in the edge regions of some of the individual droplets, indicating that solidification in these regions occurs relatively slowly after impact.



(a)



(b)

Figure 3. Highly magnified image of arc-sprayed zinc near spray center (region A in Figure 2).

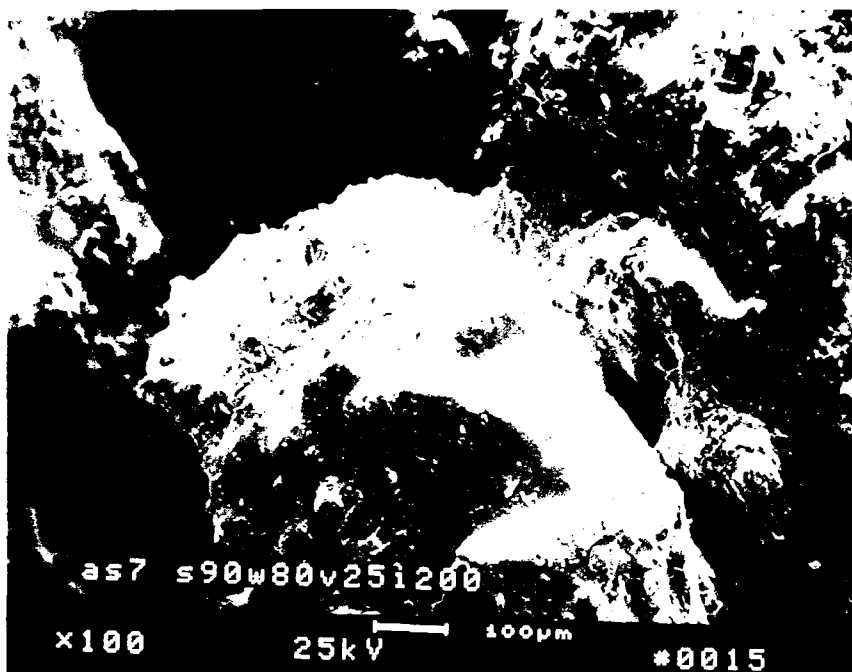


Figure 4. Highly magnified image of arc-sprayed zinc (region B in Figure 2).

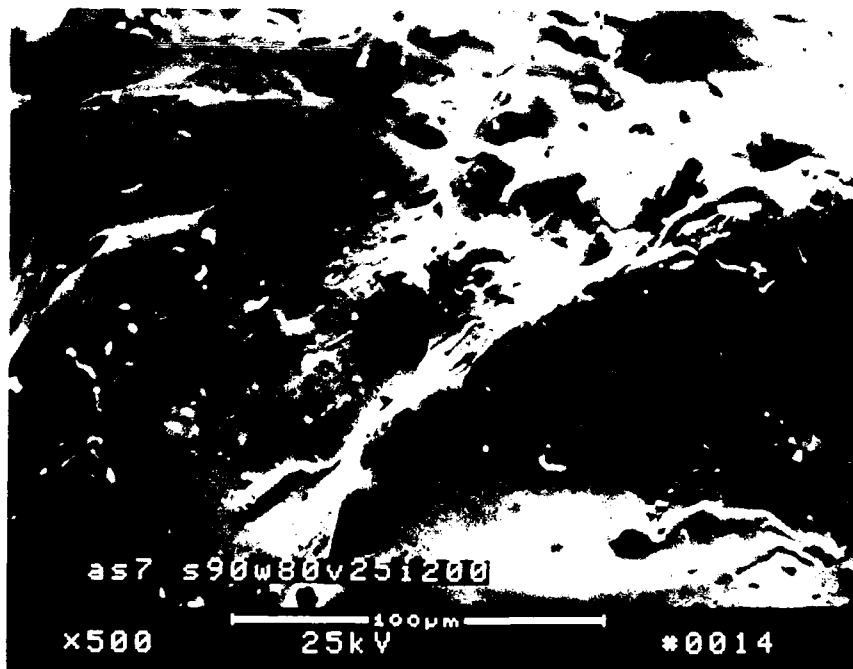


Figure 5. Highly magnified view of arc-sprayed zinc (the column in Figure 4).

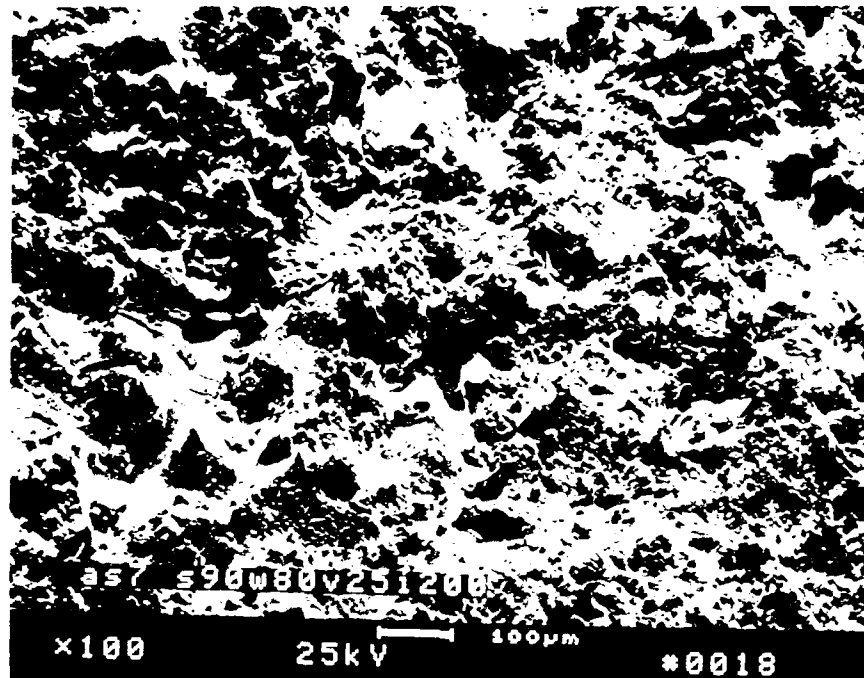


Figure 6. Highly magnified image of arc-sprayed zinc (region C in Figure 2).

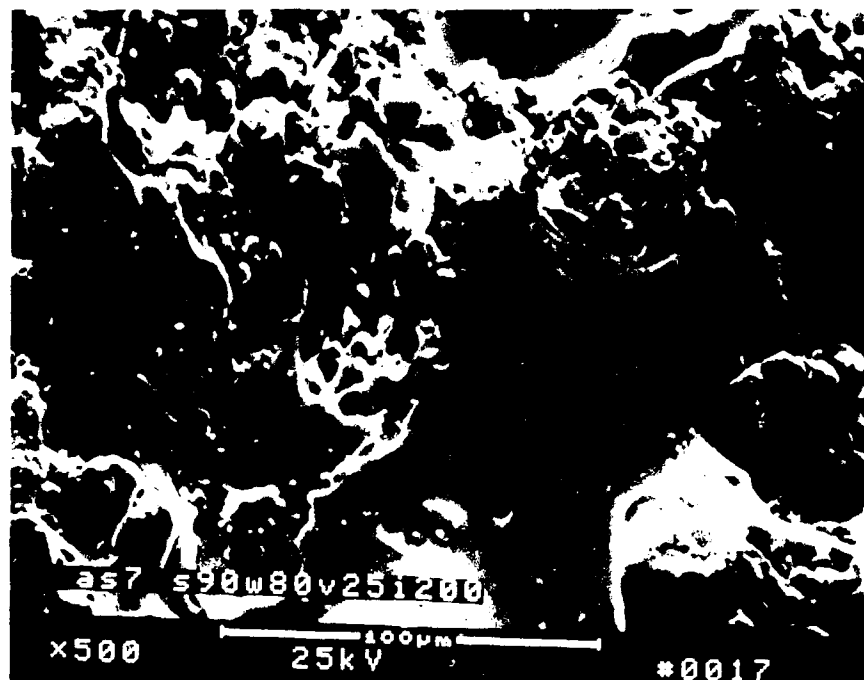


Figure 7. Highly magnified image of arc-sprayed zinc (closer view of Figure 6).

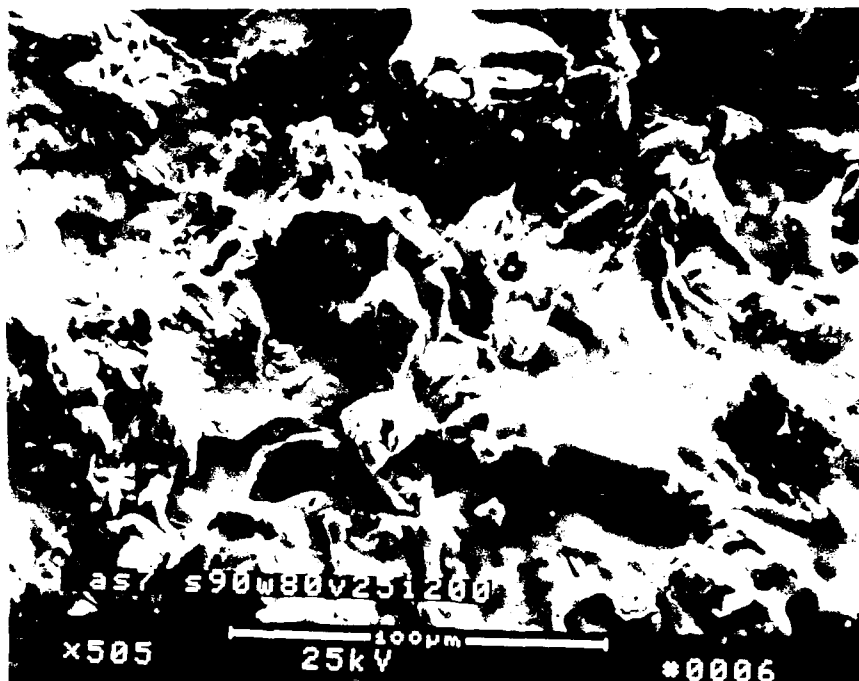


Figure 8. High magnification of arc-sprayed zinc (region D in Figure 2).

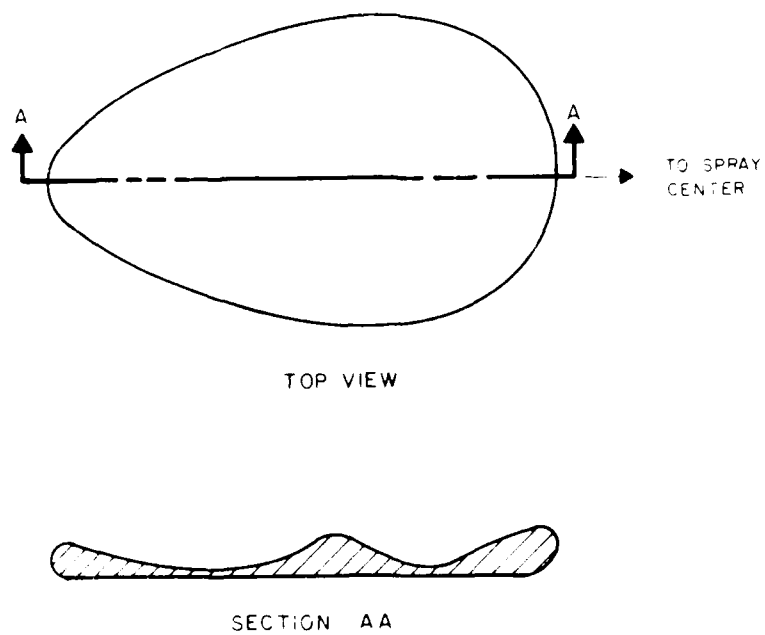


Figure 9. Deposit droplet shape.

Figure 10 is a greatly magnified image of the bottom surface of the coating away from the spray center showing the nonadherent interface. The coating in this region is not fully dense as evidenced by the roughness present. The coating here spalled off of the substrate due to thermal stresses and incomplete bonding. Bonding in this region was largely by mechanical interlocking between the droplets themselves and the substrate; since the substrate was so smooth, it did not provide adequate interlocking locations to withstand the thermal stresses generated when the coating cooled.

Figure 11 is a highly magnified view of the coating's bottom surface at a location adjacent to the spray center showing the transition from an open coating structure to a nearly fully dense structure. The aluminum foil that could not be delaminated from the coating is visible in the upper left-hand portion of the picture. Region A is the porous structure similar to that observed in Figure 10. Region B is a more dense structure, indicating complete or nearly complete coalescence between individual droplets after impact. Region C represents the transition between regions A and B. Region D is the beginning of a region of fusion between the coating and substrate. Farther toward the spray center is a region where the substrate was melted through at points and then a region where complete melting through of the substrate occurred, adjoining an area where the coating material penetrated through the molten substrate.

Figure 12 shows a cluster of deposited droplets at a large distance from the spray center for a spraying distance of 15 cm. There is evidence that the substrate topography has been reproduced in the central regions of individual droplets. Shrinkage marks are more evident at the thick outer regions of the droplets than in the thinner central regions, indicating slower cooling at the outer edges. The good conformation of droplets to existing substrate topography supports the idea that bonding occurs almost entirely by mechanical interlocking.

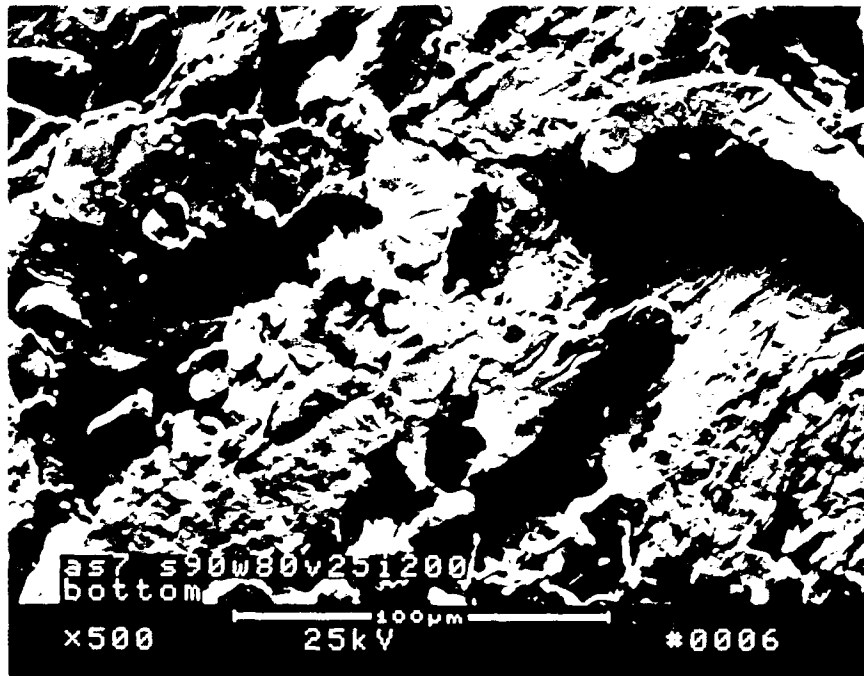


Figure 10. SEM micrograph showing interfacial surface of arc-sprayed zinc after delamination from aluminum foil substrate.

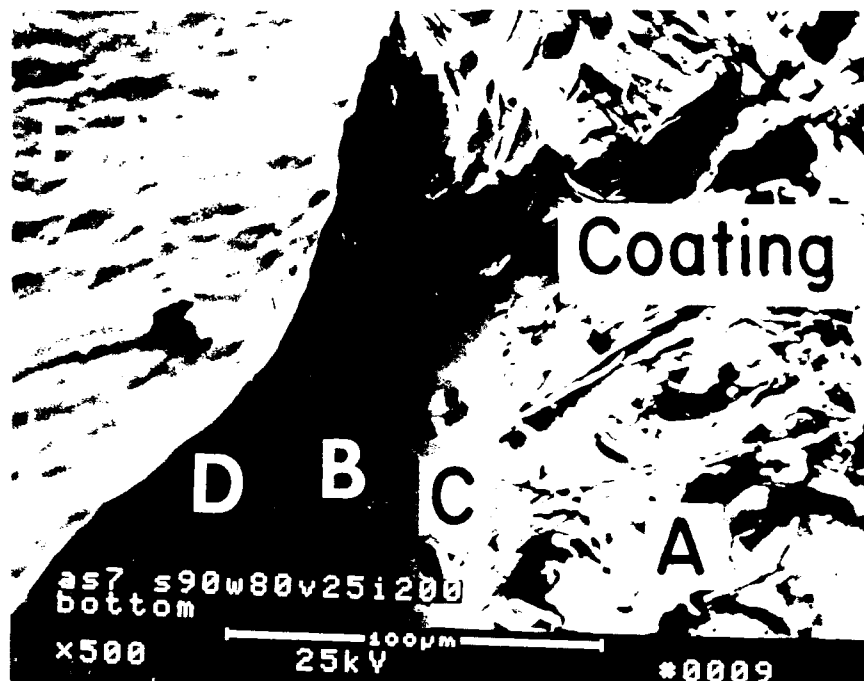


Figure 11. SEM micrograph showing bottom surface of arc-sprayed zinc coating adjacent to spray center. The boundary between good and poor bonding to aluminum foil substrate is visible.

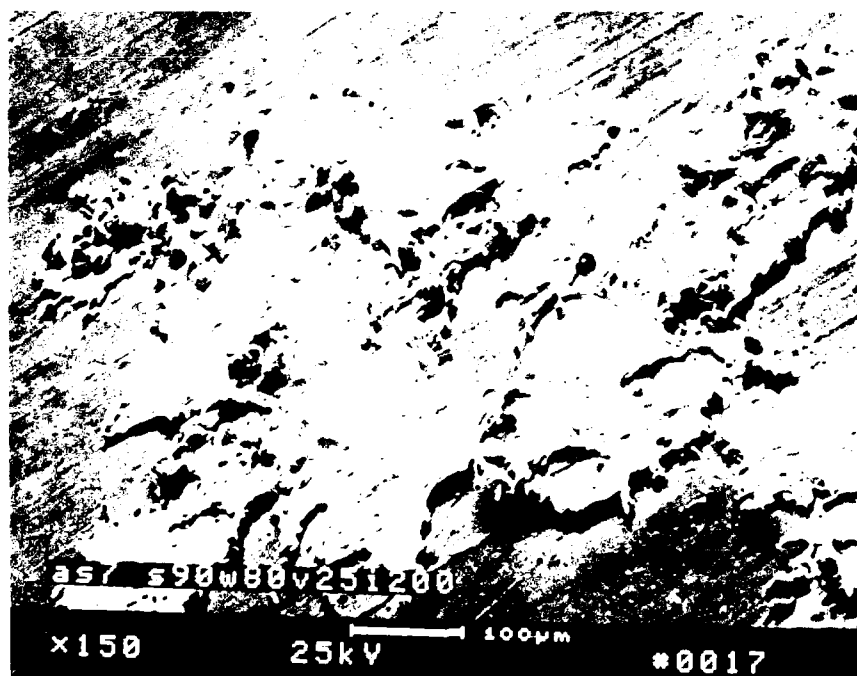


Figure 12. SEM micrograph of arc-sprayed zinc droplets deposited far from the spray center showing reproduction of substrate topography.

Figure 13 is a highly magnified view of two droplets at a large distance from the spray center. Again, the coating's conformation to the existing substrate topography is seen.

Figure 14 shows a fracture surface at a distance of about 1.91 cm from the spray center for a spraying distance of about 15 cm. The coating at this location is reasonably dense and there is some correlation between the features of the fracture surface and the substrate plane.

Figure 15 is a more highly magnified view of the same region shown in Figure 14. Ductile tearing-type fracture is evident, indicating good adhesion between individual coating particles.

Figure 16 is a high-magnification view of a fracture at a distance somewhat greater than 2.54 cm from the spray center. At this site, ductile tearing is not as evident and there is a tendency for failure due to delamination between individual particles. The cohesive strength of material in this region is clearly inferior to that of the region shown in Figure 15. Material deposited on top of this coating by multiple passes could not be expected to adhere very well to the substrate due to this weakly bonded layer.

Figure 17 is a highly magnified view of a region away from the spray center for a spray distance of 61 cm. Hail-type damage to the substrate in the area surrounding the particle is evident. The average particle size observed at this spray distance is larger than that for a spray distance of 15 cm; this finding is probably due to cooling and solidification of smaller droplets before impact, preventing them from sticking to the substrate. This condition is also suggested by the granular features present in the center of the droplet which were not visible at a spray distance of 15 cm. Also, there are no shrinkage marks, indicating that the zinc solidified very rapidly after impact.

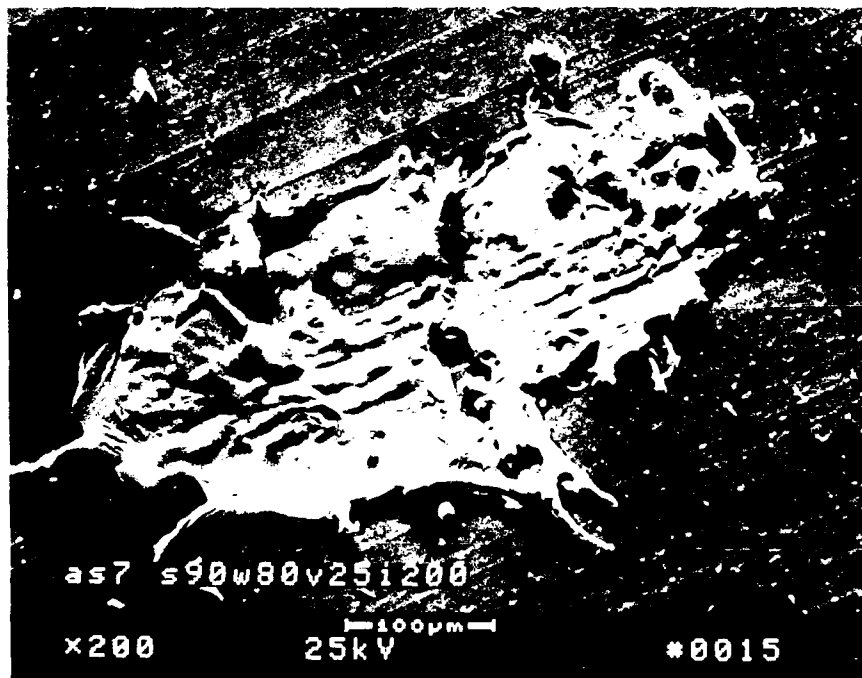


Figure 13. SEM micrograph of arc-sprayed zinc droplets showing shrinkage and conformation to substrate topography.

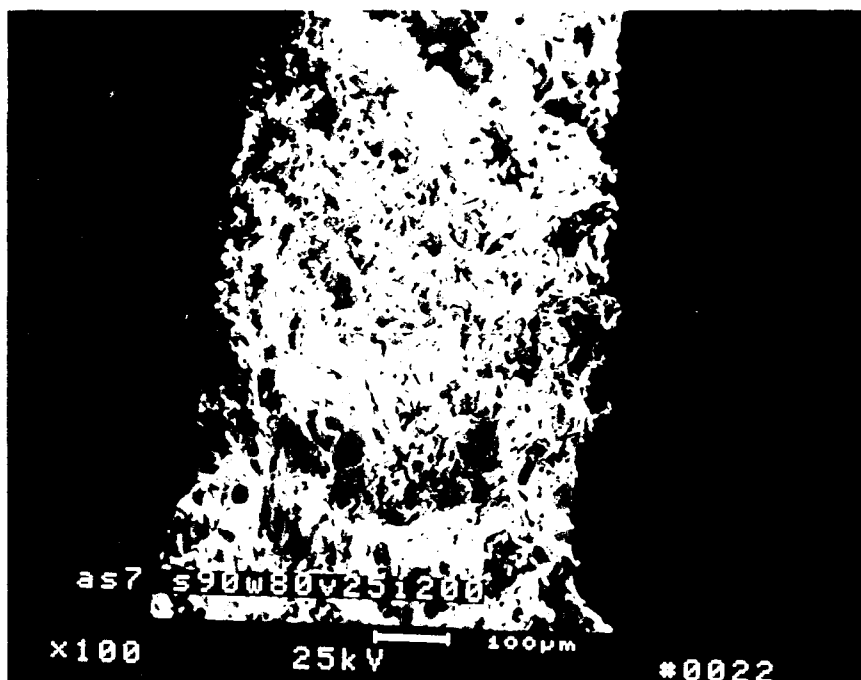


Figure 14. SEM micrograph of fracture surface in arc-sprayed zinc approximately 1.91 cm from the spray center for a spray distance of 15 cm.

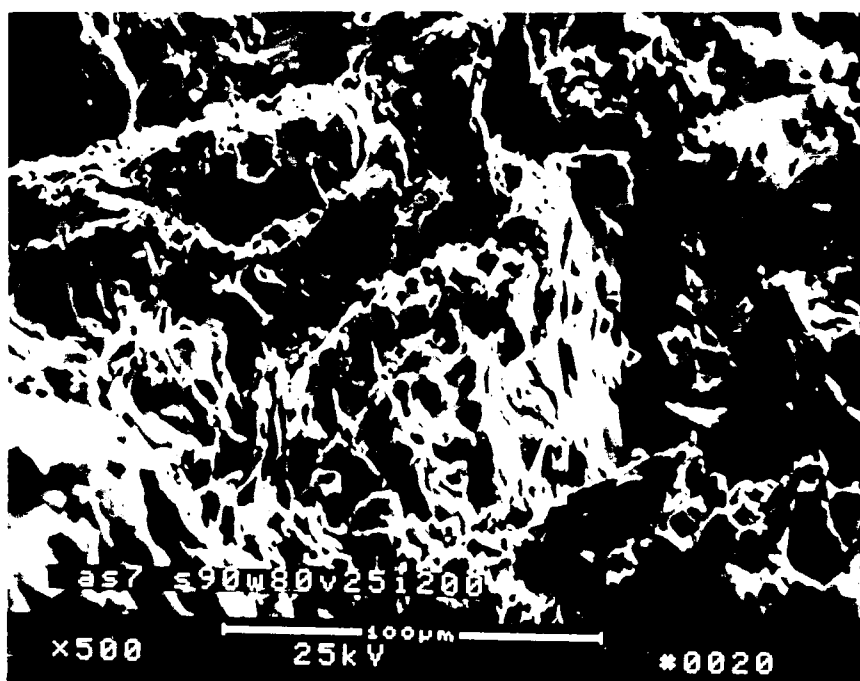


Figure 15. Higher magnification of the arc-sprayed zinc region in Figure 14.

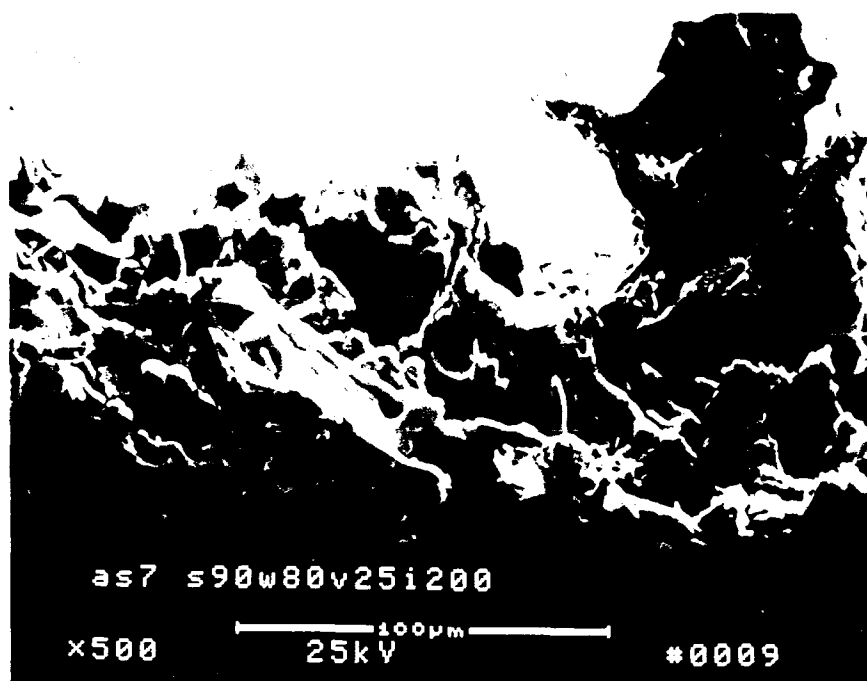


Figure 16. SEM micrograph of arc-sprayed zinc approximately 2.54 cm from the spray center for a spray distance of 15 cm.

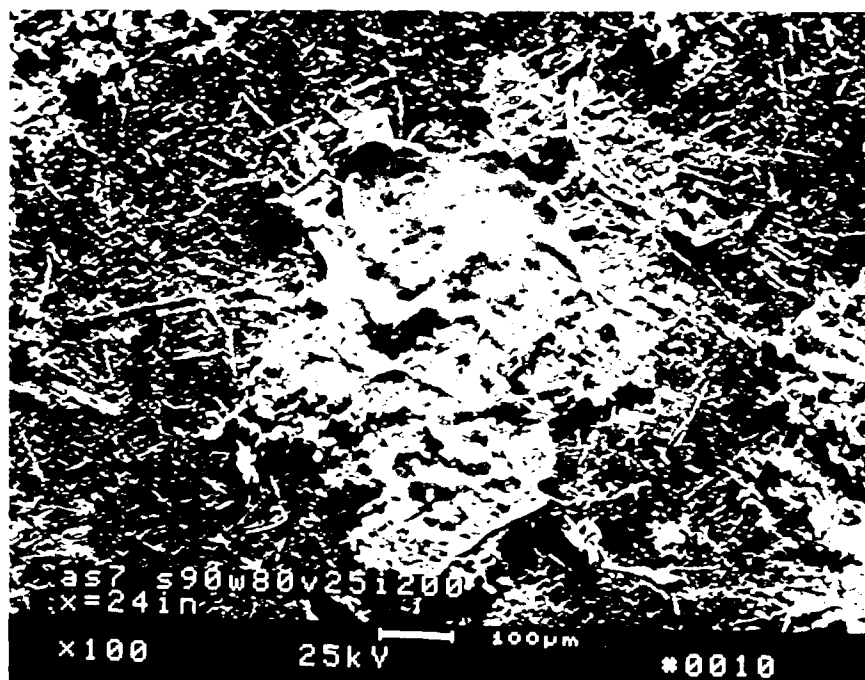


Figure 17. SEM micrograph of arc-sprayed zinc away from the spray center at a spraying distance of 61 cm.

Figure 18 shows a region similar to that in Figure 17 for a spray distance of 15 cm. Note the large number of smaller particles, indicating the droplets' nonuniform cooling rate.

Figure 19 is a micrograph of a droplet similar to those in Figure 17 at higher magnification and a spray distance of 61 cm. Note again the granular structure near the droplet center and the absence of shrinkage marks.

Figure 20 is a more highly magnified view of Figure 19. This image shows a large number of granular features.

#### *Wire Feed Rate*

Wire feed rate was measured for the zinc. Table 15 lists the results.

#### *Maximum Droplet Temperature Calculation*

The maximum possible droplet temperature was calculated by assuming that all the power in the arc is used to heat the metal and that no oxidation reactions occur. For the typical zinc spraying parameters of 25 V, 175 amps, and 0.5516 MPa wire feed pressure (about 43.7 total cm/sec), about 11.083 kcal of heat are available for each mole of material being sprayed. It takes 2.581 kcal to heat 1 mole of zinc from room temperature to its melting point and 1.595 kcal to melt 1 mole of zinc at 693 K. Another 3.655 kcal are required to heat the mole of molten zinc to its 1180 K boiling point. So far, this process has used 7.831 kcal of the available energy; the rest is used to create vapor, which takes 27.43 kcal/mole of vapor at 1180 K, resulting in 0.12 moles of vapor and 0.88 moles of liquid at 1180 K.

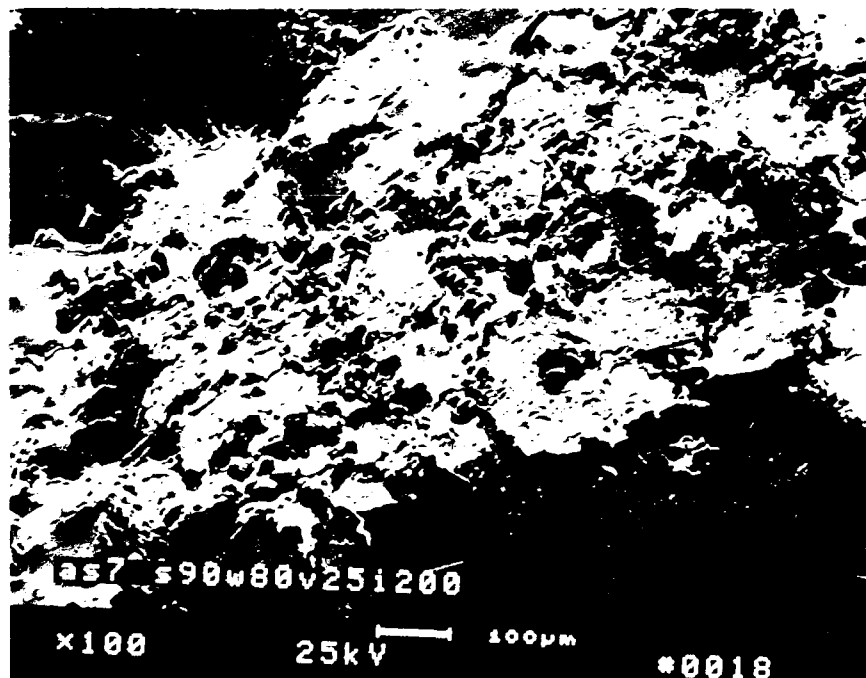


Figure 18. SEM micrograph of arc-sprayed zinc at a spray distance of 15 cm for a region similar to that in Figure 17. Many smaller particles are present.

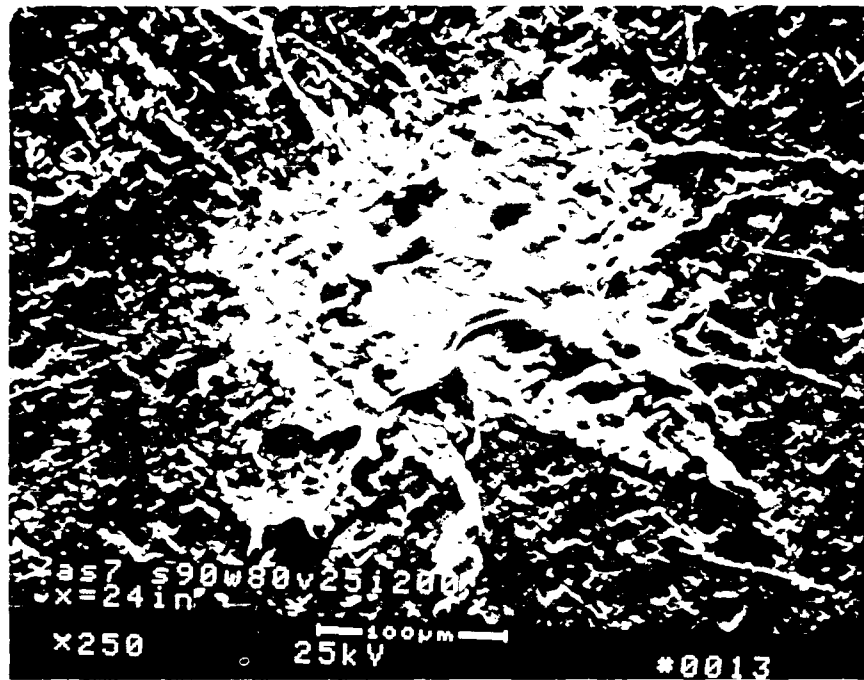


Figure 19. SEM micrograph of arc-sprayed zinc at a spraying distance of 61 cm (similar to region in Figure 17, showing greater detail).

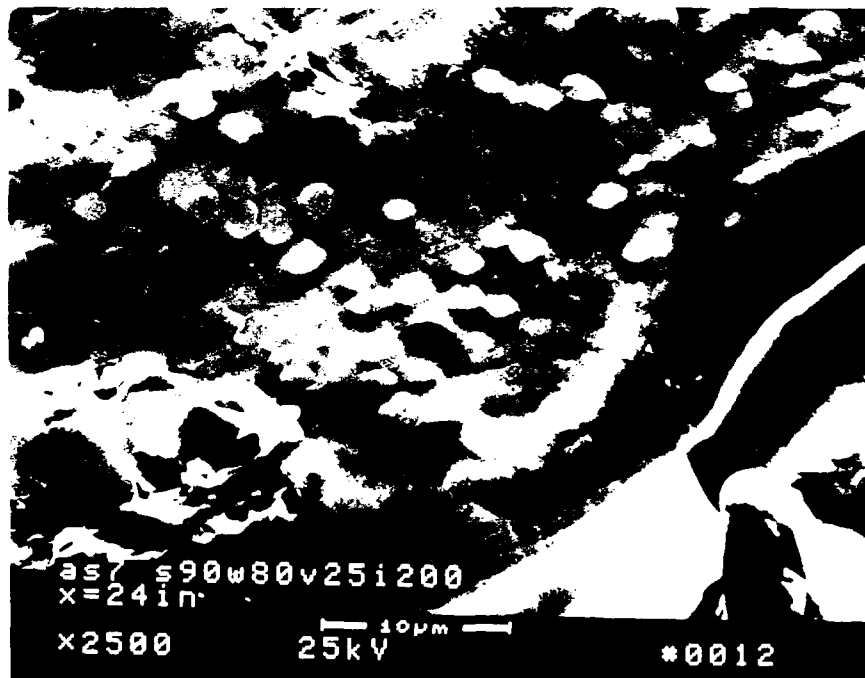


Figure 20. Detail of droplet in Figure 19 at higher magnification.

Table 15  
Wire Feed Rate for Zinc\*

wfp (MPa)	Left (m)	Right (m)	Hose**	avecm/s	tavecm/s
0.6206	5.31	5.33	b	17.74	35.46
0.6206	6.26	6.27	s	20.89	41.81
0.5516	5.17	5.18	b	17.24	34.49
0.5516	5.82	5.84	s	19.43	38.86
0.4827	4.75	4.75	b	15.83	31.65
0.4827	5.40	5.40	s	17.99	35.97
0.4137	4.18	4.19	b	13.95	27.89
0.4137	4.89	4.89	s	16.30	32.61
0.3448	3.58	3.59	b	11.96	23.93
0.3448	4.24	4.24	s	14.14	28.30
0.2758	2.84	2.87	b	9.53	19.05
0.2758	3.58	3.58	s	11.94	23.88
0.2069	2.06	2.07	b	6.88	13.77
0.2069	2.71	2.71	s	9.02	18.03
0.1379	1.00	1.00	b	3.34	6.71
0.1379	1.68	1.68	s	5.59	11.18
0.1034	0.52	0.53	b	1.76	3.51
0.1034	1.14	1.14	s	3.81	7.62
0.0690	0.05	0.05	b	0.17	0.36
0.0690	0.41	0.41	s	1.38	2.74

\*wfp = wire feed pressure; avecm/s = average cm/sec for each wire;  
tavecm/s = total average cm/sec of wire consumed during spraying.  
\*\*b = bent; s = straight.

#### *Maximum Stable Droplet Size Calculation*

The maximum stable droplet size for zinc was calculated for several spray pressures by assuming a surface tension value of 760 dynes/cm. At 0.1034 MPa,  $r$  was  $1.47 \times 10^{-3}$  cm. At 0.4137 MPa,  $r$  was  $3.67 \times 10^{-4}$  cm, and at 0.6206 MPa,  $r$  was  $2.45 \times 10^{-4}$  cm. The value for surface tension was taken from the *CRC Handbook of Chemistry and Physics*.

#### *Consumption Calculations*

The energy consumption was calculated to be about 5.06 kJ/cm<sup>3</sup> (1.41 W-hr/cm<sup>3</sup>). The material cost \$4.74/kg, or about \$0.0448/cm<sup>3</sup>. The nitrogen cost \$18 for a 8.5 m<sup>3</sup> cylinder. The discharge rate was estimated to be about 0.425 m<sup>3</sup>/min which can be converted to a nitrogen cost of \$0.0173/cm<sup>3</sup> of zinc sprayed.

## 4 SUMMARY OF FINDINGS

### Deposition Parameters

Deposition parameters for all materials sprayed were found to be within the power level allowable for 100 percent duty cycle of the sprayer. Materials with lower melting points were favored for higher wire feed rates. To cover large areas rapidly for EMP and RFI shielding, it is desirable to be able to spray the material at as high a rate as possible without causing substrate degradation. Based on these tests, the most suitable materials in terms of melting point are tin, zinc, and aluminum. However, aluminum sprayed with air was observed to oxidize exothermically, burning the paper substrates.

### Deposited Mass

The mass deposited on graph paper was measurable only for aluminum bronze, copper, iron, tin, and zinc. The other materials sprayed (aluminum, 13 percent chrome steel, nickel, and nickel-chrome) all burned through the substrate without significant deposition. In general, the deposited mass decreased as the spray distance increased. (The discussion of deposited mass in the zinc section of Chapter 3 generally applies to all the materials sprayed.)

### Deposit Efficiency

The deposition efficiency was determined for all materials that had a measurable deposited mass. The maximum deposition efficiency observed was 0.66 for zinc sprayed at 15 cm in condition AS11. Spraying at 15 cm resulted in charring of the substrate by all materials and conditions tested. Introducing relative motion between the source and substrate could perhaps reduce or eliminate this problem in many cases. Substrate charring was minimal for zinc spray at a distance of 30 cm or more. At a spray distance of 46 cm, most of the conditions used to test zinc (except AS13) gave higher deposit efficiencies than for any other materials. Low temperature (below 5 °C) during spraying appears to inhibit the deposition efficiency. The low temperature probably causes a larger number of the droplets to solidify prior to impact with the substrate than is the case for higher temperatures. In addition, lower substrate temperature increases the quench rate of the droplets and thus creates a larger thermal stress that must be accommodated to prevent droplet delamination from the substrate.

Low-power spraying conditions (AS13) that reduced droplet superheating tended to produce lower deposition efficiencies, especially at large spray distances. High-pressure spray conditions that promote finer droplet sizes generally reduced the deposition efficiency at large spray distances due to more rapid cooling of the smaller particles (enhanced surface area-to-volume ratio) and reduced droplet superheating at the source. Using nitrogen as a spray gas enhanced deposition efficiency, especially at larger spray distances where the formation of an oxide skin on the droplets would act to inhibit particle adhesion to the substrate. It can be expected that using nitrogen or another inert spray gas would improve the deposition efficiency of the other materials sprayed, as well.

In general, deposition efficiency is increased by: (1) high wire-feed rates; (2) reduced spraying pressure; (3) use of an inert spraying gas; (4) elevated environmental temperature during spraying (substrate, spray gas, atmosphere, and wire temperatures); (5) increased substrate surface roughness; (6) reduced spraying distance; (7) increased spraying time, and (8) increased spraying power as related to droplet superheating. Note: the conditions that promote deposition efficiency may also cause unwanted substrate degradation due to excessive thermal input.

## Radius of Conductivity

The ROC for all materials measured was found to increase with increasing spray distance to some maximum point, after which it decreased. For most of the materials, the optimal spray distance to maximize ROC when spraying 107 cm lengths of wire was about 46 cm. For tin, this distance was about 30 cm. Maximal conductive areas were attained by spraying zinc with conditions that enhanced deposition efficiency at large spray distances. When relative motion is introduced between the source and substrate, the optimal distance will be less to account for the motion; however, the other optimal conditions should remain similar. Shifting the spray stream for a nonnormal incidence would also increase conductive area per unit of metal sprayed; this increase, however, would be at the expense of coating adhesion.

## Radius of Opacity

The radius of opacity for all coatings sprayed was always smaller than the radius of conductivity. This finding implies that, if the coating is thick enough to be free of pinhole porosity, it will form a continuous conductive path. For the conditions used in this work, the peak in size of the opaque area was observed to occur at a spray distance of about 30 cm. Conditions that increase opaque area (aside from spray distance) appear to be the same as those that promote deposition efficiency. Details discussed in the zinc section of Chapter 3 can be extended to all of the coatings tested.

## Opacity Thickness

Opacity thickness was found to increase with increasing spray distance for all materials sprayed. This result can be explained in terms of the adhering particle size as discussed for zinc in Chapter 3.

## Bend Testing

Bend testing indicated that thicker coatings are less tolerant to bending than thin coatings.

## SEM Observations

All coatings observed showed a variation in structure from the spray center to the edge of the coating such that material near the center appeared to be denser and have a higher cohesive strength than that near the edges. This variation in structure could cause adhesive and cohesive failure of the coating--even if the coating is further built up by spray passes--since the weakest layer is at the bottom and is expected to hold the other layers to the substrate. Spraying at larger distances appeared to promote the formation of a low cohesive-strength coating away from the spray center.

There was a tendency for the adhering droplet size to increase with increasing spray distance. This finding was apparently due to cooling of smaller droplets prior to impact at larger spray distances. Higher melting point materials melted the aluminum foil at many locations away from the spray center; in contrast, zinc coatings produced localized melting of the foil only very near the spray center.

A "halo" like structure which appeared to be localized oxidation of the substrate in the region surrounding droplet impact was observed. Since adhesion is known to be inhibited by the presence of surface oxides, this observation implies that adhesion could be improved if the deposition rate were increased such that other droplets are deposited in the same region before the oxide grows to a

thickness at which it cannot be disrupted by an impacting droplet. This observation also implies that oxidation of material already deposited is further enhanced by the deposition of another particle.

### Wire Feed Rate Measurements

All materials showed an increase in wire feed rate with wire feed pressure. Also, for all materials, the wire feed rate was sensitive to bending of the wire feed tubes (radius of curvature); the percentage change due to bending was enhanced at lower wire feed pressures. At high wire feed pressures, there was some tendency for the pressure to drift due to fluctuations in the building air supply pressure. Optimally, all materials should be sprayed at as high a rate as possible with appropriate relative motion between the sprayer and the substrate to minimize the time required to coat a surface. In the case of copper, these conditions were not possible due to the high thermal conductivity and melting point of the material which required more power than the sprayer unit could supply. All materials sprayed except tin gave very few problems with wire feeding. In most cases, a wire's failure to feed properly occurred when the contact tips became worn and an arc between the tip and the wire caused the wire to fuse with the tip, allowing wire to pile up behind that point. In the case of the tin wire, tensile failure occurred due to friction with the wire feed tubes when they were in a bent position.

### Maximum Droplet Temperature Calculation

The maximum possible temperature using only the power of the arc was above the melting point of all materials sprayed except that of the low-carbon steel, which must have undergone exothermic oxidation to provide the balance of the heat required for spraying. Curiously, the temperature calculated for zinc (1180 K) was above that of tin (859 K), which implies that spraying tin, with its lower melting point (505 K), should be less destructive to organic substrates than spraying zinc with its higher melting point (693 K). Observations of coatings sprayed onto graph paper substrate indicated that this was not the case. In actuality, spraying zinc coatings onto the graph paper resulted in less charring of the paper than spraying tin. A possible explanation for this result is in the vapor pressure data (Table 16), where it can be seen that the vapor pressure of zinc is several orders of magnitude higher than any of the other materials sprayed at any given temperature. The data imply that evaporative cooling of the zinc occurs to a greater extent than for any of the other materials sprayed.

Possible advantages of zinc's high vapor pressure include:

1. A lower droplet temperature will reduce both burning of organic substrates and thermal shock to inorganic substrates, which will improve the mechanical interlocking component of adhesion since the residual stress due to thermal expansion mismatch will be reduced.
2. The vapor may act as a protective shroud around the molten droplet. This shroud may inhibit oxide film formation (which is known to inhibit adhesion) on the droplet surface by the surrounding atmosphere. This possibility is supported by the observation that the deposition efficiency of zinc is higher than that of all the other materials sprayed.
3. Oxidation of the emitted vapor may locally deplete the surrounding gas of oxygen, in addition to acting as a physical barrier to bombardment of the droplet surface by oxygen in the air. Complete occlusion of atmospheric oxygen was not achieved since a further increase in deposition efficiency was observed for exclusion of atmospheric oxygen by spraying with nitrogen.
4. Zinc oxide is known to be a good absorber of UV radiation. The oxidized vapor formed may act to absorb a portion of the UV light emitted from the arc, thus reducing the hazard to the operator.

**Table 16**  
**Temperature (K) at Different Vapor Pressures**

Element	Vapor Pressure (mm Hg)									
	$1 \times 10^{-8}$	$1 \times 10^{-6}$	$1 \times 10^{-4}$	1	10	100	400	760	1520	7600
Aluminum	950	1094	1283	1813	1053	2353	2593	2740	2883	3323
Copper	--	--	--	--	2143	2463	2713	2873	3033	3733
Iron	1131	1271	1453	2053	2313	2643	2893	3023	3173	3633
Nickel	1200	1345	1535	2073	2363	2643	2893	3003	3153	3573
Tin	955	1080	1270	1883	2163	2543	2853	3023	3223	3813
Zinc	400	450	523	--	863	1003	1113	1180	1243	1453

A possible disadvantage of the high vapor pressure is that the more rapid evaporative cooling may cause particles to solidify at a rapid enough rate to inhibit particle adhesion at larger spray distances. The deposition efficiency data indicate that inhibition of deposition efficiency by oxide film formation is probably more significant than that for cooling at large spray distances since (1) the deposition efficiency for zinc was higher than for all other materials and (2) using nitrogen as a spray gas improved this efficiency further.

#### Maximum Stable Droplet Size Calculation

The radii of the calculated maximum droplet size based on surface tension were all within about an order of magnitude of each other for all materials at any given pressure.

#### Consumption Calculations

Table 17 lists results of the consumption calculations. From the table, it is clear that the material cost varied greatly among the wires and that the energy consumed was a very small part of the cost (assuming \$0.10/kWh or \$0.0001/W-hr). The data indicate that, for spraying at 46 cm (where the size of the conductive area formed is maximal), zinc is the lowest cost material to spray, even when using nitrogen as a spraying gas. Use of nitrogen when spraying zinc at 46 cm raised the cost 5 percent and gave a 32 percent increase in deposition efficiency.

**Table 17**  
**Material Consumption and Cost**

Wire	Energy (W-hr/cm <sup>3</sup> )	Material (\$/cm <sup>3</sup> )	Deposition Efficiency (DEatx=46 cm)	Sprayed Metal (\$/cm <sup>3</sup> )
Al	1.97	0.0146	0.00	---
Al bronze	8.64	0.0910	0.08	1.1375
Cu	6.91	0.0561	0.11	0.5100
LC steel	2.23	0.0313	0.00	---
Cr steel	2.33	0.0615	0.00	---
Ni	3.11	0.2149	0.00	---
NiCr	3.19	0.1705	0.00	---
Sn	0.41	0.2368	0.19	1.2463
Zn(air)	1.41	0.0448	0.25	0.1792
N2(Zn)	--	0.0173		
N2+Zn	1.41	0.0621	0.33	0.1882

## 5 CONCLUSIONS AND RECOMMENDATIONS

This study has evaluated the physical and electrical properties of nine metals that were arc-sprayed onto different substrates to determine the optimal conditions for spraying to effect EMP shielding and military structures. The results have shown that:

1. The distribution of deposited coating structures varies radially outward from the spray center; this outcome has significant effects on the mechanical and electrical properties of the coating.

2. The deposition efficiency is a strong function of the spraying distance and a weaker function of the other sprayer parameters. Increasing the wire feed rate and voltage tends to increase efficiency at all spray distances and reducing the spray pressure promotes efficiency at larger spray distances.

3. There is an optimal spraying distance to maximize the area of the conductive and opaque regions formed. This distance increases with increasing spray time and is maximum for conditions with the highest deposition efficiency.

4. Not all of the material in the deposit has good cohesive and adhesive strength; there is a tendency for material deposited away from the spray center to be inferior to that deposited near the spray center. Material deposited on top of these coatings probably would not have good adhesive strength.

5. The distribution in particle and pore sizes in the coatings varies with spray distance and distance from the spray center; this finding suggests that one viscosity grade of epoxy for adhesion testing will not be adequate since there will be nonuniform penetration of the coatings.

6. The deposition efficiency is a function of spraying time, which also indicates that the deposition efficiency is a strong function of substrate surface roughness.

7. Use of nitrogen as a spraying gas increased the deposition efficiency and the size of the conductive areas formed.

8. Temperature of the surroundings during spraying has a significant effect on the coating deposition such that better performance is achieved when spraying on warm days than on cold days.

9. Zinc was found to give the best overall performance and cost-effectiveness.

It is recommended that these findings be used to direct further research into optimal spraying conditions. This research would be limited to zinc, which appears to have a high potential for success in EMP shielding. Specifically:

1. Work should be conducted to determine the effects of motion parameters (traverse speed, spray distance, interpass distance) on the properties of zinc coatings.

2. A mechanism to control relative motion between the spray gun and the substrate should be constructed or purchased. Keeping in mind the difficulties experienced with fluctuations in wire feed rate due to flexure of the wire feed tubes, it is recommended that the device move the substrate

relative to the spray gun. In using a robot to spray a room, flexure of the wire feed tubes will be unavoidable so that another control must be developed to accommodate this condition.

3. It is suggested that a detailed study be conducted to determine the influence of the more loosely bonded material away from the spray center on the adherence of material deposited by the next successive traverse.

4. Further work should be done to evaluate the effects of using an inert spraying gas in conjunction with controlled relative motion between the sprayer and substrate.

## CITED REFERENCES

- Nielsen, P., *Electromagnetic Shielding of Full-Sized Structures by Metal Arc Spraying*, Technical Report M-332/ADA132883 (U.S. Army Construction Engineering Research Laboratory [USACERL], August 1983).
- Weast, R. C., and M. J. Astle (Eds.), *CRC Handbook of Chemistry and Physics*, 63rd ed. (CRC Press, 1982-83).

## UNCITED REFERENCES

- Alden, J. E., and J. M. Kane, *Design of Industrial Ventilation Systems*, 5th Ed. (Industrial Press, 1982).
- American Society for Metals (ASM) Handbook Committee, *Metals Handbook, Volume 2, Properties and Selection: Nonferrous Alloys and Pure Metals*, 9th ed. (ASM, 1979).
- American Welding Society (AWS), *Rapporteurs Report and Seminar Papers of the Eighth International Thermal Spraying Conference* (1976).
- American Zinc Institute, "Furniture Life Guaranteed by Sprayed Zinc Coating," *Welding Journal* (December 1966).
- ASTM Standard B 117, "Standard Method of Salt Spray (Fog) Testing," *ASTM Annual Book of Standards* (1988).
- ASTM Standard B 571, "Standard Test Methods for Adhesion of Metallic Coatings," *ASTM Annual Book of Standards* (1988).
- ASTM Standard C 633, "Standard Test Method for Adhesion or Cohesive Strength of Flame-Sprayed Coatings," *ASTM Annual Book of Standards* (1988).
- Bailey, J. C., "Corrosion Protection of Welded Steel Structures by Metal Spraying," *Metal Construction* (May 1983).
- Batten, J. H., "Stress Profiles in Rail-Gun Projectiles with Distributed Armatures," *J. Appl. Phys.*, Vol 56, No. 11 (1 December 1984).
- Cullison, A., "Thermal Spraying Sparks Artist's Imagination," *Welding Journal* (July 1985).
- "Electromagnetic Guns: Beyond Hypervelocity," *Army* (July 1987).
- Foulke, D. G., and F. E. Crane (Ed.), *Electroplaters' Process Control Handbook* (Van Nostrand Reinhold, 1963).
- Gartner, F. W., "Corrosion Prevention With Thermal Sprayed Zinc and Aluminum Coatings," *Welding Journal* (June 1974).

- Graneau, P., "Application of Ampere's Force Law to Railgun Accelerators," *J. Appl. Phys.*, Vol 53, No. 10 (October 1982).
- Hauser, D., P. A. Kammer, and J. H. Dedrick, *Welding Research Supplement* (January 1967).
- Hermanek, F. J., "Determining the Adhesive/Cohesive Strength of Thin Thermally Sprayed Deposits," *Welding Journal* (November 1978).
- Hulst, A. P., and C. Lasance, "Ultrasonic Bonding of Insulated Wire," *Welding Journal* (February 1978).
- Joshi, K. C., *Welding Journal* (December 1971).
- Kawase, R., M. Kureishi, and K. Machara, *Transactions of the Japan Welding Society (J. W. S.)*, Vol 15, No. 2 (October 1984).
- Kelly, T. J., "Ultrasonic Welding of Cu-Ni to Steel," *Welding Journal* (April 1981).
- Kreye, H., "Melting Phenomena in Solid State Welding Processes," *Welding Research Supplement* (May 1977).
- Lieberman, E. S., "Thermally-sprayed Active Metal Coatings for Corrosion Protection in Marine Environments," MS Thesis, SUNY Stony Brook, Naval Sea Systems Command Report SUB-84-1 (January 1984).
- Longo, F. N., and G. J. Durmann, *Welding Journal* (June 1974).
- Mathewson, C. H., *Zinc: The Science and Technology of the Metal, Its Alloys and Compounds* (Reinhold, 1959).
- Meco, Inc., "Flame-Sprayed Zinc Restores Protection in Conduit Threading," *Welding Journal* (March 1969).
- Nielson, P., *Arc-Sprayed Metals for Structural Electromagnetic Shielding*, Technical Report M-316/ADA117673 (USACERL, June 1982).
- Rouse, H., *Elementary Mechanics of Fluids* (John Wiley and Sons, 1946).
- Van Horn, K. R. (Ed.), *Aluminum: Vol III. Fabrication and Finishing* (ASM, 1967).
- Wall Colmonoy Corp., "Metallizing Eliminates Maintenance in Water Tank," *Welding Journal* (June 1970).
- Wall Colmonoy Corp., "Metallizing With Tin Improves Capacitor Quality," *Welding Journal* (July 1970).
- Weiss, P. (Ed.), *Adhesion and Cohesion: Proceedings of the Symposium on Adhesion and Cohesion* (Elsevier, 1962).
- Welding Institute of Canada, *Advances in Thermal Spraying: ITSC '86 Proceedings of the Eleventh International Thermal Spraying Conference, Montreal, Canada, September 8-12, 1986* (Pergamon, 1986).

## APPENDIX:

### VARIOUS DEPOSITION PARAMETERS IDENTIFIED FOR THE STUDY

The following parameters were evaluated for potential impact on the materials under study:

- Arc voltage
- Arc current
- Wire feed rate
- Wire feed pressure
- Spray pressure
- Spray nozzle geometry
- Spray gas composition
- Ambient gas composition
- Ambient gas temperature
- Spray gas temperature
- Fume emissions
- Ultraviolet (UV) light emissions
- Characteristic light emissions from arc (wavelength will depend on arc composition; intensities will be proportional to relative amounts of the various ionized gases)
- Shroud geometry (use of side jets to produce more directed spray)
- Substrate material (e.g., melting point, decomposition temperature, thermal expansion coefficients, vapor pressure, elastic constants)
- Substrate geometry (e.g., thickness, thermal conductivity, surface preparation)
- Coating material (e.g., melting point, thermal expansion coefficients, vapor pressure, boiling point, oxidation kinetics, elastic constants viscosity as melt, surface tension as melt)
- Machine peculiarities (e.g., maximum power, inductance)
- Nugget cooling rate
- Extent of coating oxidation
- Wire geometry (cross section--circular, rectangular)
- Spray distance
- Interpass distance
- Interpass time
- Distance from spray center
- Spraying time
- Elastic constants of wire as related to friction in feed tubes
- Friction in feed tubes varied as a result of bending during spraying
- Material constants of oxide formed during spraying (e.g., melting point, hardness, elastic properties, softening point, fracture strength, toughness, adherence)
- Angle of incidence of particles with respect to substrate surface
- Flow rate of spraying gas
- Dewpoint of ambient atmosphere
- Substrate temperature
- Spraying gas temperature
- Power supply (AC, DC, peaks and valleys; Is the arc extinguished between cycles?)
- Substrate heat capacity
- Substrate/coating interfacial reactions
- Coating porosity
- Coating thickness
- Deposition rate
- Deposition efficiency
- Coating electrical and magnetic properties

- Coating microstructure
- Coating adherence
- Coating coherence
- Coating corrosion properties
- Coating mechanical properties (e.g., ductility, fracture strength, elongation at failure)
- Deposit thickness distribution (varies with sprayer geometry, nozzle shape, spray pressure, spray time, material sprayed, spray distance, and other factors)
- Relative nobility of coating and substrate (will galvanic corrosion occur?)
- Coating reflectance
- Deposit cooling rate
- Maximum temperature during deposition
- Degree of superheating of droplets before leaving the arc
- Temperature of droplets on impact with substrate
- Size distribution of particles on impact with substrate
- Edge effects when spraying in corners
- Delamination properties (will a localized delamination promote further delamination due to stress effects or will it terminate locally?)
- UV reflectance of the coating (as an operator hazard during spraying)
- UV reflectance and absorption of the fume cloud during spraying
- Wear and buildup in the wire feed tips which modify the effective resistance to wire feed
- Metal dust buildup between the wire feed tubes which leads to the formation of a conductive path (short) between the electrodes
- Arc shape
- Impurities in the arc gas
- Peak arc temperature
- Contact tube-to-arc distance and the effects of "spool drag" as wire is consumed.

## USACERL DISTRIBUTION

Chief of Engineers  
ATTN: CEIM-SL  
ATTN: CEEC-EE  
ATTN: CERD

CEHSC ATTN: CEHSC-PREP 22060

US Army Engineer Districts  
ATTN: Library (41)

US Army Engr Divisions  
ATTN: Library (14)

DNA ATTN: NADS 20305

INSCOM - Ch, Instl. Div.  
Arlington Hall Station (4) 22212  
ATTN: Facilities Engineer  
Vint Hill Farms Station 22186  
ATTN: IAV-DEH

SHAPE 09055  
ATTN: Survivability Sect. CCB-OPS  
ATTN: Infrastructure Branch, LANDA

Tyndall AFB, IL 32403  
AFESC/Engineering & Service Lab

US Government Printing Office 22304  
Receiving/Depository Section (2)

Defense Technical Info. Center 22314  
ATTN: DDA (2)

US Army White Sands Missile Range  
NY 88002  
ATTN: STEWS-TE-NO-EMP

ADEA Fort Lewis, WA 98433  
ATTN: AFVO-TRA-EN

USA NATICK  
R&D Cntr 01760-5017  
ATTN: STRNC-VE/N. Roberts

Harry Diamond Labs 20783  
ATTN: DELHD-NW-E  
ATTN: DELHD-NW-EA  
ATTN: DELHD-NW-EC  
ATTN: DELHD-NW-ED  
ATTN: DELHD-NW-EE

Naval Air Systems Command  
ATTN: Library

Hanscom AFB, MA 01731  
ATTN: HQ AFSC  
ATTN: ESD/AVMS

Kirtland AFB, NM 87117  
ATTN: AFWL/DES  
ATTN: AFWL/DYC  
ATTN: AFWL/NTCA

Wright-Patterson AFB, OH 45433  
ATTN: ASD/ENAMA  
ATTN: AFWAL/MLSE

Naval Civil Engr Lab  
ATTN: Library 93041  
ATTN: Code L08A  
ATTN: Code L72  
ATTN: Code L33

National Bureau of Standards 20899

US Naval Sea Systems Command  
ATTN: PMS-423

USACC Ft Huachuca 85613  
ATTN: USAI SEIC AT ASBI-SST

Defense Nuclear Agency  
ATTN: DNA-RAEE  
ATTN: DNA-RAEV